CELL BIOLOGY

# CLIC4 localizes to mitochondrial-associated membranes and mediates cardioprotection

**Devasena Ponnalagu[1,2], Shanna Hamilton[1,2]†, Shridhar Sanghvi[1,2]†, Diego Antelo[1,2], Neill Schwieterman[1,2,3], Inderjot Hansra[1], Xianyao Xu[2,4], Erhe Gao[5], John C. Edwards[6], Shyam S. Bansal[1,2], Loren E. Wold[1,2,3], Dmitry Terentyev[1,2], Paul M. L. Janssen[1,2], Thomas J. Hund[2,4], Mahmood Khan[2,7], Andrew R. Kohut[8], Walter J. Koch[5], Harpreet Singh[1,2]***



**Mitochondrial-associated membranes (MAMs) are known to modulate organellar and cellular functions and can subsequently affect pathophysiology including myocardial ischemia-reperfusion (IR) injury. Thus, identifying molecular targets in MAMs that regulate the outcome of IR injury will hold a key to efficient therapeutics. Here, we found chloride intracellular channel protein (CLIC4) presence in MAMs of cardiomyocytes and demonstrate its role in modulating ER and mitochondrial calcium homeostasis under physiological and pathological conditions. In a murine model, loss of CLIC4 increased myocardial infarction and substantially reduced cardiac function after IR injury. CLIC4 null cardiomyocytes showed increased apoptosis and mitochondrial dysfunction upon hypoxia-reoxygenation injury in comparison to wild-type cardiomyocytes. Overall, our results indicate that MAM-CLIC4 is a key mediator of cellular response to IR injury and therefore may have a potential implication on other pathophysiological processes.**

## INTRODUCTION

A growing body of evidence implicates mitochondrial-associated membranes (MAMs) in regulating various cellular processes and act as signaling nanodomains of reactive oxygen species (ROS) and calcium ($Ca^{2+}$) (*1*, *2*) between the endoplasmic reticulum (ER) and mitochondria. Any dysregulation in the function of MAM proteins disrupts the ER-mitochondrial coupling and communication and causes adverse effects including tumor formation, inflammation, and neurological disorders (*1*). Therefore, identifying the MAM proteins and defining their signaling mechanisms will underpin previously unidentified pharmacological therapeutic targets for several human diseases. Intracellular ion channels by maintaining ionic homeostasis are known to regulate intraorganellar communication and act as a major factor in determining cell fate (*3*). Although cation channels are being characterized in MAMs (*4*), the molecular identity and functional relevance of chloride ($Cl^-$) channels are poorly understood. The major class of intracellular chloride channels, chloride intracellular channel (CLIC) proteins, is known to regulate diverse physiological functions such as phagosome acidification, cell cycle regulation, angiogenesis, and apoptosis and has been implicated in human diseases (*5*, *6*). All six mammalian paralogs of CLICs (CLIC1 to CLIC6) can exist in both soluble and integral membrane forms and reside in different organellar membranes, but their presence in MAM is still not established (*7*). The key unanswered question remains how the soluble form of CLICs inserts into the membrane to form functional ion channels.

CLICs facilitate cardioprotection as blocking CLICs increases myocardial infarction (MI) (*8*) upon ischemia-reperfusion (IR) injury and abrogates the cardioprotective effects of ischemic preconditioning (IPC) (*9*). As a CLIC inhibitor, indanyloxyacetic acid (IAA-94) can block all the paralogs of CLIC proteins, and the precise role and mechanism of CLICs in preventing MI and their importance in human heart failure (HF) remain elusive. Our study highlights the presence of CLIC4 in MAMs, the previously unidentified role and mechanism of the MAM-specific CLIC4 in ER-mitochondrial $Ca^{2+}$ homeostasis, and cardioprotection from IR injury by modulating mitochondrial physiology. We observed a differential distribution of CLIC4 in cytosol relative to organellar membrane fractions in HF patients versus healthy hearts. As CLIC4 is important in mediating a wide array of cellular processes (*5*, *6*), our findings shed light on mechanisms by which MAM chloride channels regulate several pathophysiological conditions.

## RESULTS

### CLIC4 is a MAM $Cl^-$ channel

In mouse adult cardiomyocytes, we probed the localization and distribution of CLIC4 with respect to the organellar marker of mitochondria (MitoTracker), mitofusin 2 [outer mitochondrial membrane (OMM) and MAM] (*1*), and acyl–coenzyme A (CoA) synthetase long-chain family member 4 (ACSL4) (MAM) (*10*) (Fig. 1, A and B). CLIC4 showed a higher colocalization with the mitochondria (41.2 ± 0.6%, $n = 40$ cells) and ER-mitochondria contact site proteins mitofusin 2 and ACSL4 (34 ± 1% and 31 ± 2%, $n = 25$ cells, respectively). CLIC4 in isolated crude mitochondria (58 ± 10%) and neonatal cardiomyocytes (40 ± 4%, $n = 28$) also showed an association with MitoTracker-loaded mitochondria (fig. S1), but CLIC1, a paralog of CLIC4, showed a lower colocalization to crude mitochondria (39 ± 8%, $P = 0.03$) or neonatal cardiomyocytes (29 ± 3%, $P = 0.03$, $n = 28$) in comparison to CLIC4 (fig. S1). To establish the precise localization of CLIC4 in cardiomyocytes, we purified the mitochondria using 30% Percoll gradient centrifugation (*11*) and observed that, similar to GRP78 (ER/MAM marker), CLIC4

[1]Department of Physiology and Cell Biology, The Ohio State University, Columbus, OH, USA. [2]Dorothy M. Davis Heart and Lung Research Institute, The Ohio State University, Columbus, OH, USA. [3]College of Nursing, The Ohio State University, Columbus, OH, USA. [4]Departments of Biomedical Engineering and Internal Medicine, Dorothy M. Davis Heart and Lung Research Institute, The Ohio State University, Columbus, OH, USA. [5]Center for Translational Medicine, Department of Pharmacology, Lewis Katz School of Medicine, Temple University, Philadelphia, PA, USA. [6]Nephrology Division, Department of Internal Medicine, St. Louis University, St. Louis, MO, USA. [7]Department of Emergency Medicine, The Ohio State University College of Medicine, Columbus, OH, USA. [8]Penn Heart and Vascular Center, University of Pennsylvania, Philadelphia, PA, USA.
*Corresponding author. Email: harpreet.singh@osumc.edu
†These authors contributed equally to this work.

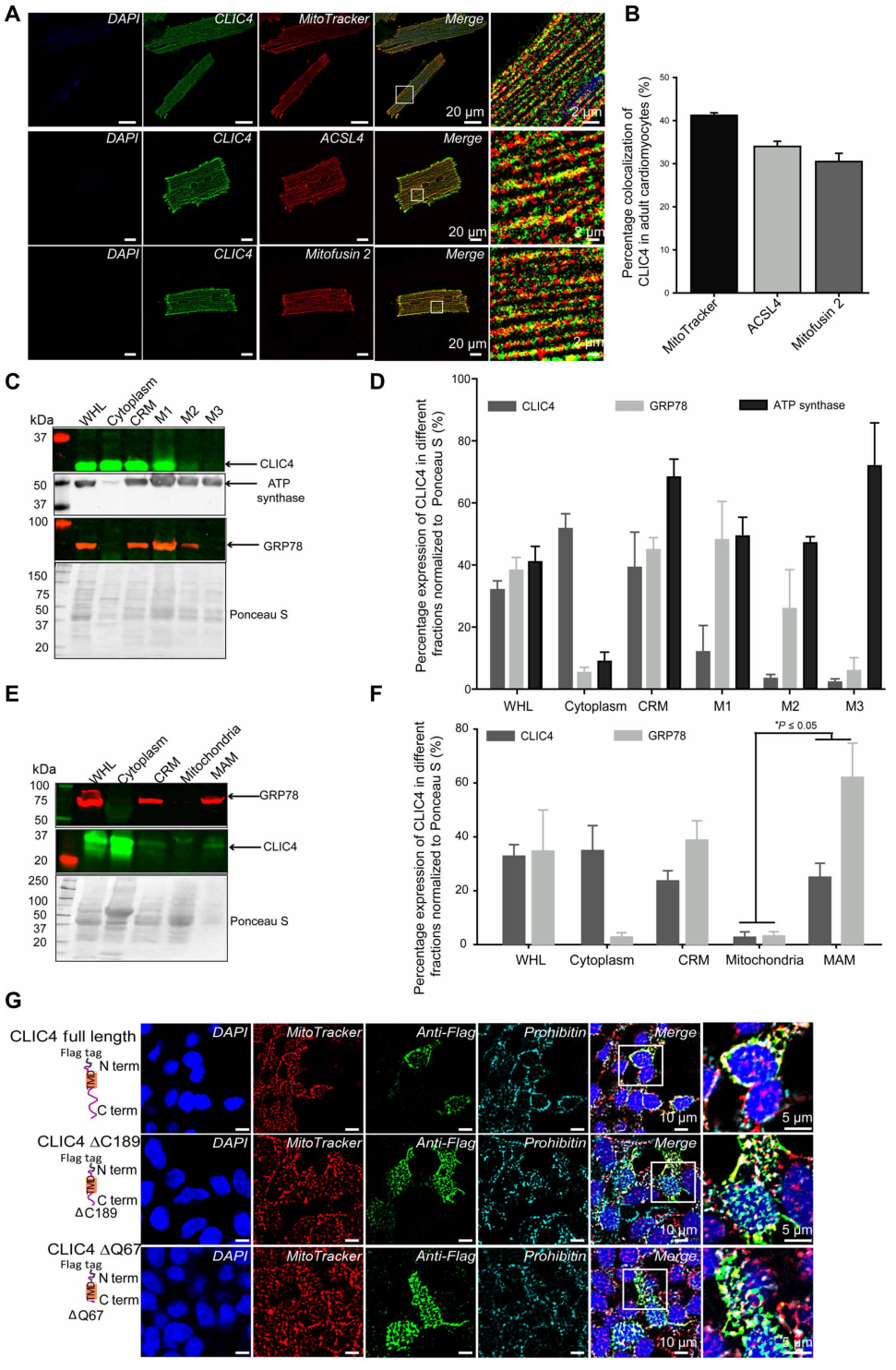


**Fig. 1. Biochemical characterization of CLIC4.** (**A**) Representative image of mouse adult cardiomyocytes loaded with MitoTracker, labeled with anti-CLIC4 antibody, anti-ACSL4, and anti–mitofusin 2, and costained with DAPI shows colocalization of CLIC4 to mitochondria (row 1), ACSL4 (row 2), and mitofusin 2 (row 3). (**B**) Bar graph showing quantification of the colocalization. Data are represented as mean ± SEM; $N = 4$ isolation; $n \geq 25$. (**C**) Representative Western blot showing fractionation profile of ultrapure mitochondria (M3) indicating the absence of CLIC4 and GRP78 in M3 fraction but the presence of ATP synthase in M3 fraction. (**D**) Quantification of percentage expression of CLIC4, GRP78, and ATP synthase normalized to total protein as detected by Ponceau S staining in different subcellular fractions. (**E**) Representative Western blot of MAM fractionation indicates the presence of CLIC4 in MAM but their absence in purified mitochondria. (**F**) Quantification of percentage expression of CLIC4 and GRP78 normalized to total protein content estimated by Ponceau S stain in various subcellular fractions. The graph in (D) and (F) depicts mean ± SEM for percentage normalized expression of the proteins; $N = 3$; $^*P \leq 0.05$, Student's $t$ test. (**G**) HEK cells transfected with CLIC4 full-length FLAG (row 1), CLIC4ΔC189 (row 2), and CLIC4ΔQ67 (row 3) were loaded with MitoTracker, anti-FLAG antibody, and anti-prohibitin antibody and costained with DAPI, showing colocalization of all CLIC constructs to mitochondria (Merge).

presence was negligible in ultrapure M3 fraction (Fig. 1, C and D) (*12*). The absence of CLIC4 in ultrapure mitochondria and their high degree of colocalization to MitoTracker-loaded cardiomyocytes prompted us to assess their presence in MAMs. Western blot analysis and its quantification indicated a preferential distribution of CLIC4 to MAMs rather than ultrapure mitochondrial fraction, establishing CLIC4 as a MAM-specific $Cl^-$ channel (Fig. 1, E and F).

We also examined the domain of CLIC4 involved in targeting them to MAMs. We transfected human embryonic kidney (HEK) cells with N-terminal FLAG-tagged constructs of full-length CLIC4, CLIC4-ΔC189, in which the C-terminal domain of CLIC4 was partially truncated, and CLIC4-ΔQ67, which retained the N terminus and the transmembrane domain (TMD) (*13*). Our results demonstrate that each transfected CLIC4 construct colocalized to MitoTracker in HEK cells (Fig. 1G), thus indicating that the N terminus with intact TMD is responsible for its targeting and localization to MAMs.

## MAM-CLIC4 modulates $Ca^{2+}$ homeostasis

MAMs are contact sites for $Ca^{2+}$ and ROS signaling between ER and mitochondria (*1*, *2*, *14*). To understand the role of MAM-CLIC4 in $Ca^{2+}$ signaling, we transduced mouse neonatal cardiomyocytes (MNCMs) of wild-type (wt) and *clic4*$^{-/-}$ pups [postnatal day 3 (p3)] with adenovirus encoding the organelle-targeted $Ca^{2+}$ sensors G-CEPIA1er (*15*) [ER/sarcoplasmic reticulum (SR); Fig. 2A] and mtRCamp1h (*16*)

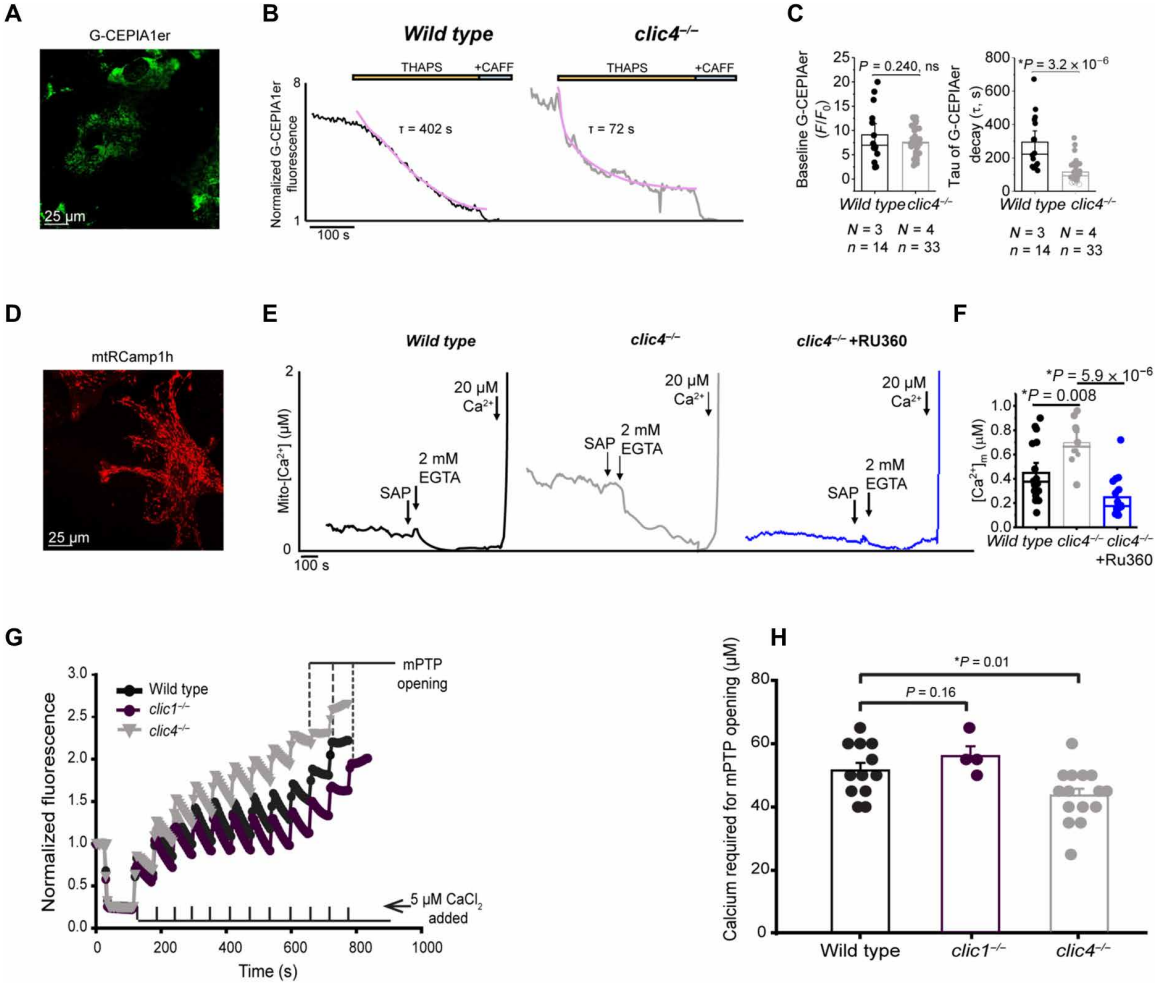


**Fig. 2. Functional characterization of CLIC4.** (**A**) Representative image of cultured MNCMs 72 hours after adenoviral infection with G-CEPIA1er intra-SR $Ca^{2+}$ biosensor. (**B**) Representative time-dependent profiles ($F/F_0$) of G-CEPIA1er fluorescence from infected MNCMs. Myocytes were exposed to SERCA inhibitor thapsigargin (THAPS; 10 μM) after 2 min of recording, and the time constant of decay (τ, s) was calculated as a measure of SR $Ca^{2+}$ leak. Signal was normalized to minimum fluorescence obtained by application of high-dose caffeine (10 mM). (**C**) The graph depicts mean data ± SEM for baseline G-CEPIA1er fluorescence ($F/F_0$) and tau (s). $N = 3$ wt isolations, $N = 4$ *clic4*$^{-/-}$ isolations, $n = 14$ wt MNCMs, $n = 33$ *clic4*$^{-/-}$ MNCMs. *$P < 0.05$, Student's *t* test. (**D**) Representative image of cultured MNCMs 72 hours after adenoviral infection with mtRCamp1h matrix $Ca^{2+}$ biosensor. (**E**) Representative traces of $[Ca^{2+}]_m$ (μM) of wt and *clic4*$^{-/-}$ MNCMs, as well as *clic4*$^{-/-}$ MNCMs preincubated with Ru360 (1 μM) for 10 min. After 5 min of recording, MNCMs were saponin–permeabilized (SAP) before treatment with EGTA (2 mM) to obtain minimum fluorescence, followed by $Ca^{2+}$ (20 μM) to obtain maximal fluorescence. (**F**) The graph depicts mean data ± SEM for $[Ca^{2+}]_m$ (μM). $N = 3$ isolations for wt, $N = 3$ isolations for *clic4*$^{-/-}$, $n = 18$ wt MNCMs, and $n = 11$ *clic4*$^{-/-}$ MNCMs. *$P < 0.05$, Student's *t* test. (**G**) Extramitochondrial $Ca^{2+}$ is labeled with $Ca^{2+}$ Green-5N, and the uptake of $Ca^{2+}$ is measured in *wt*, *clic4*$^{-/-}$, and *clic1*$^{-/-}$ cardiac mitochondria, by addition of 5 μM $CaCl_2$ pulses. mPTP activates when the maximum threshold of $Ca^{2+}$ is reached within mitochondria. (**H**) Bar graph representing quantification of average pulses of $CaCl_2$ required for mPTP opening. $Ca^{2+}$ required for mPTP opening is represented as mean ± SEM; $N = 12$ wt, $N = 4$ *clic1*$^{-/-}$, and $N = 15$ *clic4*$^{-/-}$; *$P < 0.05$, Student's *t* test.

(mitochondria; Fig. 2D) 48 to 72 hours before measuring SR and mitochondrial $Ca^{2+}$ changes, respectively. To measure SR $Ca^{2+}$ leak, $Ca^{2+}$ uptake via SR/ER $Ca^{2+}$–adenosine triphosphatase (SERCa2a) was blocked by thapsigargin, and the time constant of decay of G-CEPIA1er fluorescence was used as an indicator of SR $Ca^{2+}$ leak. The time constant of decay of G-CEPIA1er fluorescence was relatively faster in *clic4*$^{-/-}$ in comparison to wt MNCMs, suggesting an accelerated SR $Ca^{2+}$ leak in *clic4*$^{-/-}$ cardiomyocytes (Fig. 2, B and C). Moreover, we also observed increased mitochondrial $Ca^{2+}$ in *clic4*$^{-/-}$ MNCMs (Fig. 2, E and F) in comparison to wt as indicated by increased mtRCamp1h fluorescence. The increased mitochondrial $Ca^{2+}$ in *clic4*$^{-/-}$ MNCMs was reverted in the presence of mitochondrial calcium uniporter (MCU), inhibitor Ru360 (Fig. 2, E and F) (*17*). The faster SR $Ca^{2+}$ leak and increased mitochondrial $Ca^{2+}$ levels indicate defective SR and mitochondrial $Ca^{2+}$ homeostasis in *clic4*$^{-/-}$ MNCMs. $Ca^{2+}$ overload in mitochondria is known to trigger mitochondrial permeability transition pore (mPTP) opening, leading to cell death (*18*). Therefore, we measured $Ca^{2+}$ retention capacity (CRC) in wt and *clic4*$^{-/-}$ cardiac mitochondria. CRC is the ability of mitochondria to retain $Ca^{2+}$ in the matrix until threshold levels are reached, eventually leading to mPTP opening. Briefly, extra mitochondrial $Ca^{2+}$ was labeled with $Ca^{2+}$ Green-5N, and CRC was determined by the addition of $CaCl_2$ pulses. *Clic4*$^{-/-}$ cardiac mitochondria exhibited reduced CRC in comparison to wt cardiac mitochondria (~17%, $P = 0.01$, $n > 11$) signifying an early onset of mPTP opening (Fig. 2, G and H) and increased susceptibility to stress. In contrast, the absence of ER-specific CLIC1 (*19*) showed CRC similar to wt cardiac mitochondria (Fig. 2, G and H), indicating the specific role of MAM-localized CLIC4 but not ER-associated CLIC1 in regulating the mPTP opening. The expression of MCU and mPTP regulatory protein cyclophilin D (fig. S2, A and B) (*8*) was similar in *clic4*$^{-/-}$ and wt cardiac tissue. Cyclosporin A (CsA) ((*8*), an inhibitor of cyclophilin D, was able to enhance CRC in both wt (~2-fold) and *clic4*$^{-/-}$ (~2-fold) cardiac mitochondria in comparison to the respective vehicle controls. However, CRC in *clic4*$^{-/-}$ cardiac mitochondria in the presence of CsA (93 ± 7.3%) was still notably lower than that in CsA-treated wt cardiac mitochondria (130 ± 7.6%, $P = 0.025$, $n = 3$) (fig. S2, C and D).

Next, we evaluated changes in mitochondrial and cytoplasmic $Ca^{2+}$ simultaneously to study caffeine-induced ER to mitochondrial $Ca^{2+}$ transfer in wt versus *clic4*$^{-/-}$ cardiomyocytes. To measure mitochondrial $Ca^{2+}$, MNCMs were transduced with mtRCamp1h-expressing adenovirus and cytosolic $Ca^{2+}$ was measured using Fluo-3 AM. Caffeine was used to induce RyR2-mediated $Ca^{2+}$ release in cardiomyocytes. As shown in Fig. 3 (A and B), we observed a substantial reduction in cytosolic caffeine transient amplitude in *clic4*$^{-/-}$ cardiomyocytes in comparison to wt cardiomyocytes, indicating increased SR-$Ca^{2+}$ leak in *clic4*$^{-/-}$ cardiomyocytes due to hyperactive RyR2 channels. Mitochondrial caffeine transient amplitude was similar in both wt and *clic4*$^{-/-}$ cardiomyocytes upon caffeine induction, indicating more efficient $Ca^{2+}$ transfer at lower cytosolic [$Ca^{2+}$] available for uptake in these cardiomyocytes (Fig. 3, C and D). Together, our results establish the importance of MAM-CLIC4 in maintaining $Ca^{2+}$ homeostasis at the ER/SR-mitochondrial interface.

We also evaluated the role of CLIC4 in cytosolic $Ca^{2+}$ handling. Adult wt and *clic4*$^{-/-}$ cardiomyocytes were loaded with Fluo-3 AM, and cytosolic $Ca^{2+}$ transients were induced by pacing at 0.5 Hz and were recorded in the presence and absence of β-adrenergic receptor stimulation using isoproterenol (ISO) (100 nM). There were no

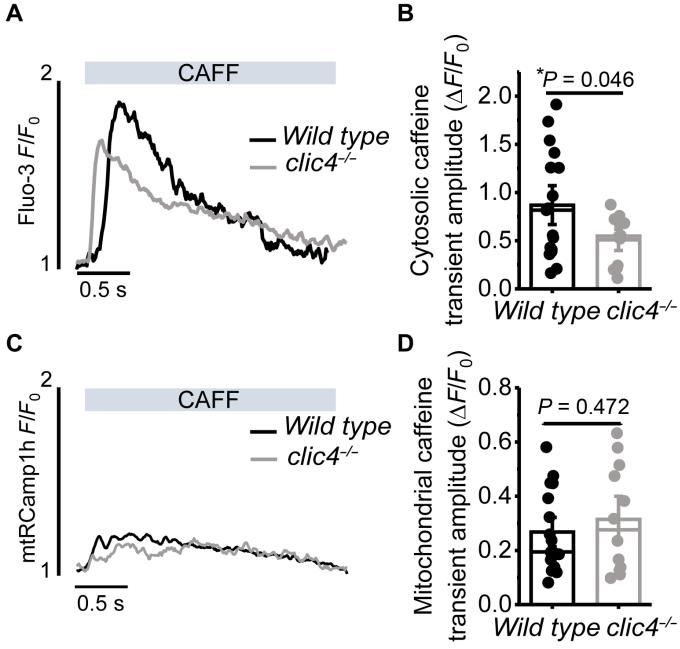


**Fig. 3. CLIC4 affects ER/SR-mitochondrial $Ca^{2+}$ transfer.** (**A**) Fluo-3 fluorescence ($F/F_0$) profiles of wt and *clic4*$^{-/-}$ MNCM cytosolic $Ca^{2+}$ transient induced by high-dose caffeine. (**B**) Mean data ± SEM for $Ca^{2+}$ transient amplitude. $n = 12$ *clic4*$^{-/-}$ cells, $n = 17$ wt cells, and $N = 3$ isolations per group. (**C**) mtRCamp1h fluorescence profiles of caffeine-induced $Ca^{2+}$ transient, with graphs in (**D**) representing mean ± SEM. $n = 17$ wt cells, $n = 12$ *clic4*$^{-/-}$ cells, and $N = 3$ isolations per group (same cells as I and II). *$P < 0.05$, Student's *t* test.

changes observed in the $Ca^{2+}$ transient amplitude, time to peak, and rate of SERCa2a $Ca^{2+}$-mediated uptake in the presence and absence of ISO in wt versus *clic4*$^{-/-}$ cardiomyocytes (fig. S3, A to H). At the end of the experiment, caffeine was added to measure SR $Ca^{2+}$ content. We did not observe changes in the caffeine transient amplitude in the presence and absence of ISO in wt versus *clic4*$^{-/-}$ cardiomyocytes. Cytosolic $Ca^{2+}$ changes were also detected using Fura-2AM staining in the presence and absence of ISO (*20*). In agreement, we did not observe any alteration in the $Ca^{2+}$ transient amplitude (Δ340/380) in *clic4*$^{-/-}$ cardiomyocytes, indicating no changes in the cytosolic $Ca^{2+}$ transients (fig. S3, I and J). Thus, our study highlights that the absence of CLIC4 is not sufficient to overcome the self-regulatory capacity of $Ca^{2+}$ handling machinery to alter cytoplasmic $Ca^{2+}$ cycling in adult cardiomyocytes (fig. S3, A to J).

## Ablation of CLIC4 enhances MI upon IR injury

Dysregulation of $Ca^{2+}$ homeostasis in cardiomyocytes has been associated with HF and MI (*21*, *22*). Moreover, blocking $Cl^-$ channels, including CLIC4, using IAA-94 augmented MI upon IR injury (*8*) and prevented cardioprotective effects of IPC (*9*). To ascertain the pathophysiological role of CLIC4, we compared the extent of myocardial injury in age-matched wt and *clic4*$^{-/-}$ mice upon left main descending coronary artery (LCA) ligation (*23*). The absence of CLIC4 significantly exacerbated the infarct size (43 ± 3%, $N = 5$, $P = 0.03$) in comparison to wt mice (28 ± 3%, $N = 5$) as evaluated by Evans blue and 2,3,5-triphenyl tetrazolium chloride (TTC) double-stained cardiac sections (Fig. 4, A and B). The probable ischemic area as defined by the area at risk (AAR) in percent of total myocardium was similar across all the groups (Fig. 4C). After LCA ligation,

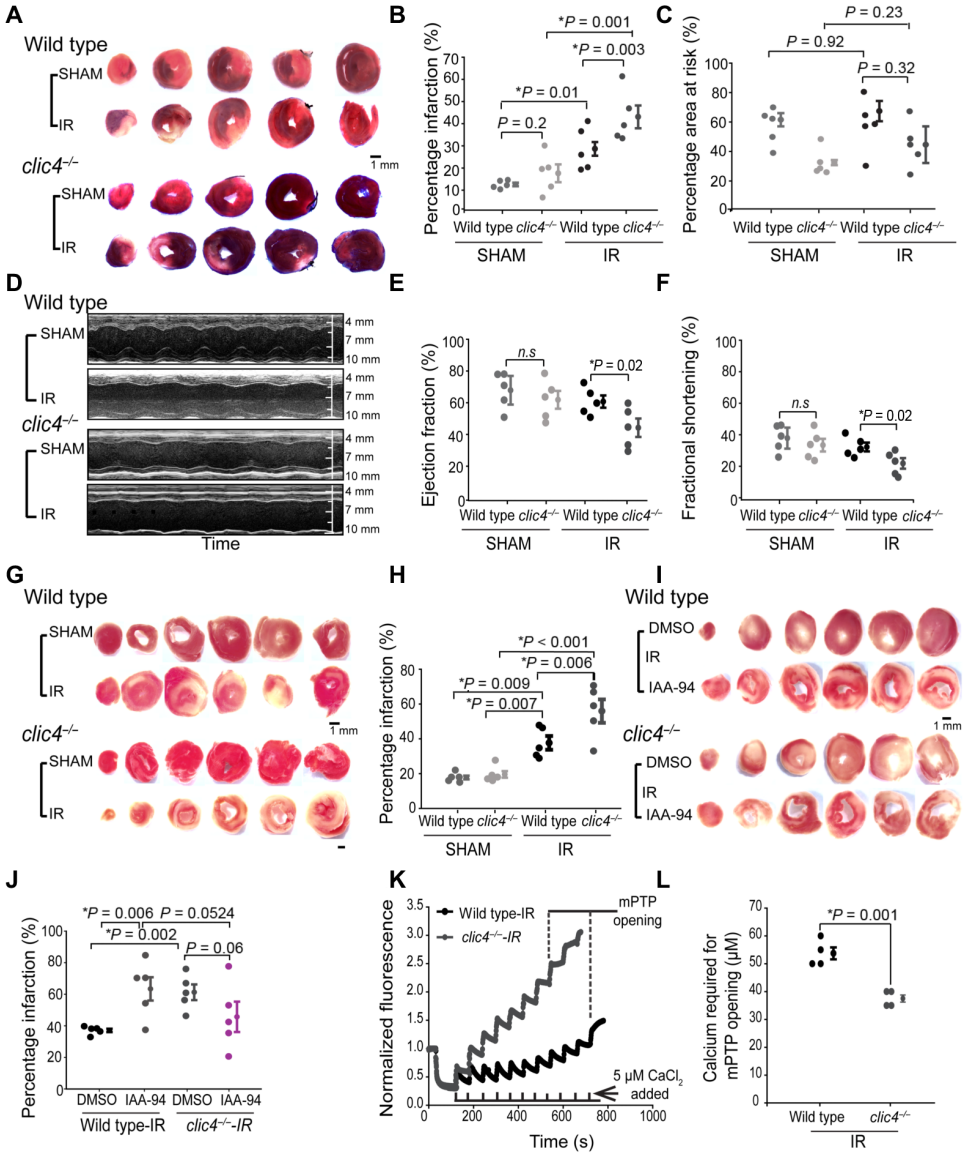


**Fig. 4. CLIC4 is required for cardioprotection from IR injury.** (**A**) Mice subjected to LCA ligation for 40 min and reperfusion for 24 hours showed increased infarction in cardiac section of *clic4*$^{-/-}$ mice in comparison to wt. Sham controls did not present any infarction. (**B**) Graph representing infarction size normalized to the AAR. (**C**) The AAR was similar in the different experimental groups. (**D**) Representative M mode echocardiographic image of wt and *clic4*$^{-/-}$ left ventricle after 24 hours of sham and IR surgery. Both LVEF (**E**) and fractional shortening (**F**) were notably reduced in *clic4*$^{-/-}$ mice after IR injury in comparison to wt mice. (**G**) TTC-stained cardiac section of wt and *clic4*$^{-/-}$ hearts after Langendorff-based ex vivo IR injury shows increased infarction in *clic4*$^{-/-}$ hearts. (**H**) Quantification of infarction after sham and ex vivo IR injury. (**I**) After global ischemia of 25 min, IAA-94/DMSO was perfused for 10 min before reperfusion in hearts of wt and *clic4*$^{-/-}$ mice. Representative cardiac sections stained with TTC show a significant increase in infarction in wt hearts in the presence of IAA-94, but such increase was not observed in *clic4*$^{-/-}$ hearts. (**J**) Quantification of infarct size in the presence or absence of IAA-94 in wt and *clic4*$^{-/-}$ hearts. (**K**) CRC profile of wt and *clic4*$^{-/-}$ cardiac mitochondria after ex vivo IR injury. (**L**) Bar graph representing quantification of average pulses of $CaCl_2$ required for mPTP opening is significantly lower in *clic4*$^{-/-}$ cardiac mitochondria upon ex vivo IR injury. Data are depicted as mean ± SEM; $N = 5$ for each experimental group; *$P < 0.05$, Student's *t* test.

*clic1*$^{-/-}$ mice showed similar myocardial infarct size as wt hearts (fig. S4, A to C), emphasizing that CLIC4, but not CLIC1, is involved in cardioprotection from ischemic events in the heart. As expected, the plasma troponin levels after IR injury were increased in both groups of mice subjected to IR injury in comparison to sham surgeries (fig. S4F). Echocardiography analysis (Fig. 4, D to F) (*24*, *25*) demonstrated no differences in the left ventricular ejection fraction (LVEF) and left ventricular fractional shortening (LVFS) between *clic4*$^{-/-}$ and wt mice, respectively, after 24 hours of sham surgeries. However, in the IR groups, *clic4*$^{-/-}$ hearts showed impaired and akinetic anterior wall motion in comparison to wt hearts (Fig. 4D and movies S1 to S4). After IR injury, LVEF and LVFS in *clic4*$^{-/-}$ were found to be 44 ± 6% (Fig. 4E) and 22 ± 3% (Fig. 4F), respectively, whereas wt mice showed LVEF of 60 ± 4% and LVFS of 32 ± 3% ($N = 5$ each in wt and *clic4*$^{-/-}$, respectively). There was a substantial reduction in left ventricular function in *clic4*$^{-/-}$ mice after IR injury in comparison to wt mice, indicating that CLIC4 expression is vital to maintain cardiac function ($P = 0.02$, $N = 5$). On the

contrary, *clic1*$^{-/-}$ mice showed LVEF and LVFS similar to those of wt mice after IR injury (fig. S4, D and E).

We also investigated the role of cardiac CLIC4 in an ex vivo IR injury model using Langendorff perfused heart assay (*12*). In agreement with the results obtained in in vivo IR injury model (Fig. 4, A to F), we observed a significant increase in the extent of MI in *clic4*$^{-/-}$ hearts in comparison to that of wt (56 ± 7% versus 38 ± 4%, $P = 0.02$, $N = 5$) as determined by TTC staining (Fig. 4, G and H). The sham control of *clic4*$^{-/-}$ and wt mice hearts showed a similar level of infarction (~18%, $N = 5$ each). IAA-94 increased MI in wt mice in comparison to the vehicle control [dimethyl sulfoxide (DMSO)] (37 ± 1% versus 63 ± 7%, $P \leq 0.05$, $N = 5$) (Fig. 4, I and J) but not in *clic4*$^{-/-}$ hearts (61 ± 5% versus 46 ± 10%, $N = 5$) after ex vivo IR injury, suggesting CLIC4 as a specific target of IAA-94 in the heart. Furthermore, after ex vivo IR injury, the $Ca^{2+}$ required for mPTP opening in *clic4*$^{-/-}$ cardiac mitochondria (37.5 ± 1.3%) was significantly reduced in comparison to wt cardiac mitochondria (53.8 ± 2.1%, $P = 0.001$, $N = 4$) (Fig. 4, K and L). This confirms that the absence of CLIC4 increases MI in *clic4*$^{-/-}$ mice by regulating mitochondrial $Ca^{2+}$ as demonstrated previously (Fig. 2). Our results provide empirical evidence to attribute cardiac CLIC4 as a novel player in protecting the heart from ischemic insults and also as a key target for IAA-94–mediated cardio-deleterious effects.

HF is associated with changes in ion channel expression, their distribution, and function (*26*, *27*). CLIC4 expression was enhanced in the lungs of pulmonary arterial hypertension patients (*28*) and in patients suffering from rheumatic heart valvular disease (*29*). We probed the expression changes of CLIC4 in cardiac sections of mouse hearts subjected to 8 weeks of permanent LCA ligation and in HF patients. Cardiac sections of mice exposed to chronic myocardial injury showed an increase in the expression of CLIC4 ($P < 0.01$, $N = 4$) relative to that of sham-operated mice (fig. S5, A and B). Such augmented expression of CLIC4 was also observed in cardiac sections of HF patients in comparison to those of nonfailing hearts (fig. S5, C and D). As CLICs are known to change their distribution upon stress (*30*, *31*), we sought to determine the distribution of CLIC4 and CLIC1 in failing and nonfailing hearts. As shown in fig. S5 (E and F), although not significant, an increase in the distribution of CLIC4 was observed in cytosol relative to an organellar fraction (*32*) in failing hearts in comparison to nonfailing hearts. However, no changes in the distribution of CLIC1 were observed. This suggests that in HF, decreased insertion of CLIC4 to organellar membrane fraction affects its ion channel function and thereby plays a crucial role in cardioprotection.

### Cardiomyocyte CLIC4 is involved in cellular protection

We also examined the cardioprotection mediated by CLIC4 at the cellular level in MNCMs independent of other cardiac cell milieu. *Clic4*$^{-/-}$ MNCMs subjected to 6 hours/12 hours of hypoxia-reoxygenation (HR) injury exhibited enhanced cell death in comparison to wt (24 ± 8% versus 4 ± 0.4%, $P < 0.05$, $N = 3$) as detected by increased TUNEL (terminal deoxynucleotidyl transferase–mediated deoxyuridine triphosphate nick end labeling)–positive cells (Fig. 5, A and B) (*33*), suggesting a role for CLIC4 in determining cardiomyocyte response to HR injury. Mitochondrial membrane potential ($\Delta\Psi_m$) is a key determinant of cell viability (*34*). Loss of $\Delta\Psi_m$ upon mPTP opening is well established to induce MI (*34*). Because decreased CRC was noted in *clic4*$^{-/-}$ cardiac mitochondria, we measured loss of $\Delta\Psi_m$ in the wt and *clic4*$^{-/-}$ MNCMs after HR injury using potentiometric dye JC1 (*33*). *Clic4*$^{-/-}$ MNCMs exhibited a reduction of $\Delta\Psi_m$, by 26 ± 5% relative to normoxia ($P \leq 0.05$, $N = 4$, $n = 500$ cells), while wt showed $\Psi_m$ loss by only 7 ± 2%, suggesting a key role of CLIC4 in maintaining $\Delta\Psi_m$ (Fig. 5, C and E). Increased mitochondrial ROS generation and $Ca^{2+}$ overload are the major factor governing mPTP opening leading to cell death (*18*). *Clic4*$^{-/-}$ MNCMs subjected to HR injury exhibited a remarkable increase in ROS generation relative to normoxia (1.4 ± 0.1–fold, $N = 4$, $n = 500$ cells), whereas wt showed only a 1.1 ± 0.04–fold increase (Fig. 5, D and F). These results highlight the prominent role of CLIC4 in mediating cellular protection upon HR injury by regulating ROS and mPTP opening.

## DISCUSSION

Here, we establish CLIC4 as a novel $Cl^-$ channel present at the MAMs. There are 1212 proteins identified in MAMs, of which 1000 have been characterized in the brain and liver (*4*, *35*, *36*). A few of these proteins are ion channels that are deemed important for regulating $Ca^{2+}$ homeostasis between ER and mitochondria (*4*). As ion channels play a crucial role in determining the structural and functional integrity of the cell and organelles, their tightly regulated functions are imperative to mediate ER-mitochondrial communication. Besides SERCA2a and RyR2, sodium ($Na^+$) and potassium ($K^+$) channels are also reported in MAMs (*4*). However, the identity of equally important $Cl^-$ channels in cardiac MAMs and their potential role in regulating MAM functions are not yet deciphered. In this study, we systematically reveal the presence of intracellular $Cl^-$ channel protein, CLIC4, in cardiac MAMs but not in mitochondria. In addition, we established that the N-terminal region with the intact TMD is essential and sufficient to retain its localization in MAMs. CLIC4 (also known as p64H1, mtCLIC, and HuH1) is shown to be distributed in mitochondria (*19*, *37*, *38*) and ER (*39*), and upon cellular stress conditions, it can translocate to the nucleus (*31*). Our results further highlight the differential distribution of CLIC4 in mouse cardiomyocytes.

The discovery of CLIC4 in MAMs prompted us to examine its physiological roles. The distance between ER and mitochondria ranges between 10 and 25 nm (*40*), and thus, it is not surprising that they are spatially and functionally coupled together. ER-mitochondrial interactions are implicated in ROS and $Ca^{2+}$ transport between them (*41*, *42*). We observed a rapid $Ca^{2+}$ release in cardiomyocytes in the absence of CLIC4, indicating SR $Ca^{2+}$ leak. This suggests a possible regulatory role of CLIC4 on $Ca^{2+}$ release channels like IP3Rs and RyR2s (*43*). Previously, it was shown that the activity of RyR2s can be modulated by the anionic gradient observed in SR (*44*). Another CLIC family member, CLIC2, which is absent in mice (*7*), is known to regulate the activity of skeletal muscle RyR1 by modulating their open probability by inducing the conformational change in them (*45*). Similar to these results, we demonstrate a role of CLIC4 in modulating the activity of RyR2 in mouse cardiomyocytes. Consequently, it would be interesting to investigate the mechanism by which CLIC4 modulates RyR2 activity.

We also observed an enhanced basal mitochondrial $Ca^{2+}$ in neonatal *clic4*$^{-/-}$ cardiomyocytes. Furthermore, this increased basal mitochondrial $Ca^{2+}$ could be responsible for reduced CRC in *clic4*$^{-/-}$ cardiac mitochondria. However, in *clic4*$^{-/-}$ hearts, we did not observe any changes in the expression of MCU, a protein responsible

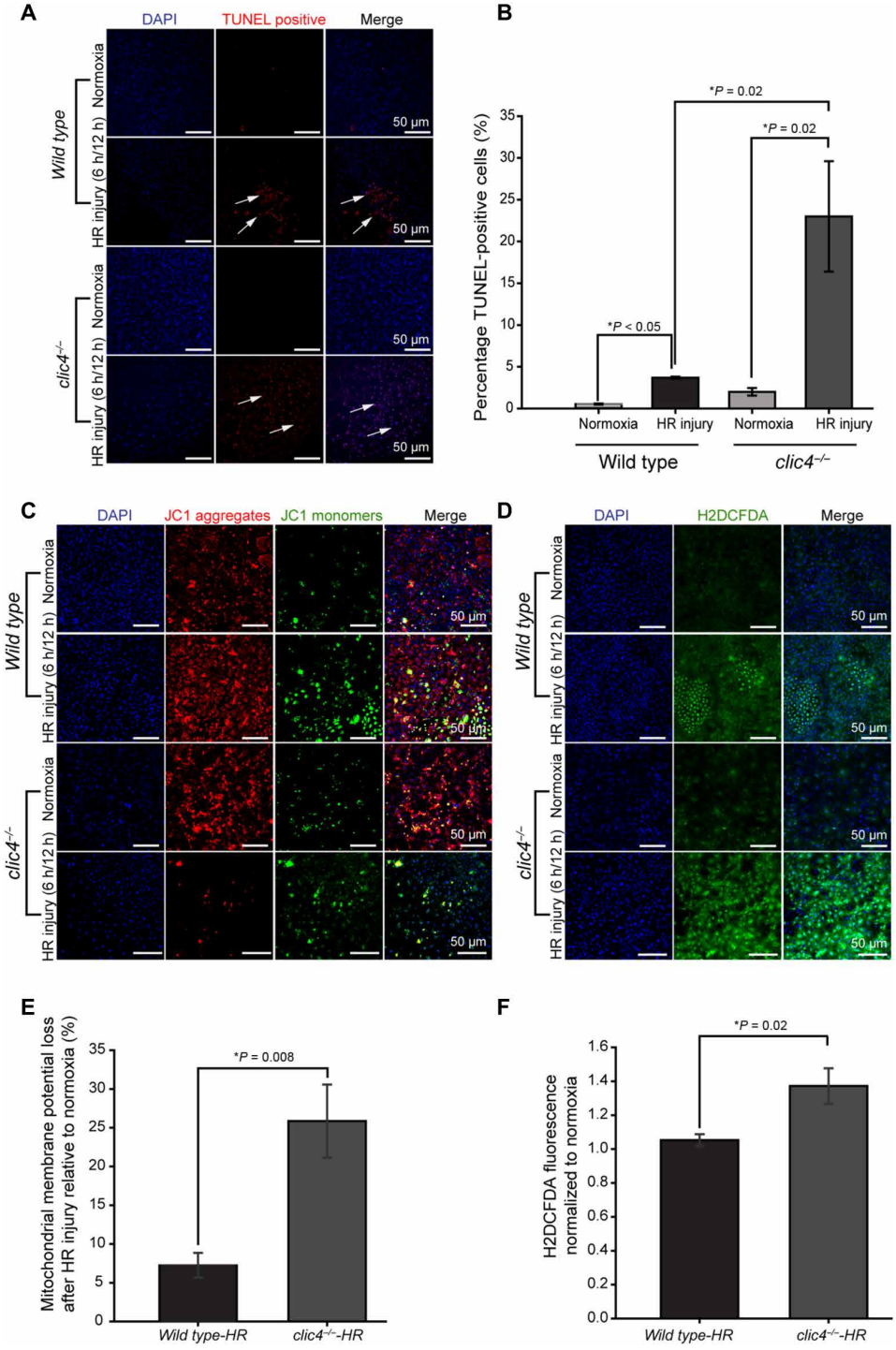


**Fig. 5. CLIC4 mediates cellular protection from HR injury by regulating mitochondrial membrane potential and ROS levels.** (**A**) MNCMs isolated from wt and *clic4*$^{-/-}$ pups were subjected to 6 hours of hypoxia and 12 hours of reoxygenation. Cells were fixed and stained for TUNEL-positive nuclei (red) and nucleus (blue). Arrows indicate TUNEL-positive cells. (**B**) Quantification of TUNEL-positive cells. Data are represented as percentage TUNEL-positive cell mean ± SEM. $N = 3$ isolations, $n = 1000$ cells for both wt and *clic4*$^{-/-}$ cardiomyocytes. *$P < 0.05$, by one-way analysis of variance (ANOVA) test with Newman-Keuls post hoc analysis. (**C**) Representative confocal images of JC1 uptake by MNCMs isolated from wt and *clic4*$^{-/-}$ p3 pups, subjected to HR injury and cultured in normoxia conditions. (**D**) Confocal images of H2DCFDA stained wt and *clic4*$^{-/-}$ MNCMs after HR injury and cultured in normoxia condition. (**E**) Bar graph representing increased mitochondrial membrane potential loss relative to normoxia in *clic4*$^{-/-}$ cardiomyocytes after HR injury in comparison to wt MNCMs. Data are represented as percentage mitochondrial membrane potential loss mean ± SEM. $N = 4$ isolations and $n = 500$ cells for both wt and *clic4*$^{-/-}$ cardiomyocytes; *$P < 0.05$, by one-way ANOVA test with Newman-Keuls post hoc analysis. (**F**) Bar graph showing increased ROS production relative to normoxia in *clic4*$^{-/-}$ MNCMs in comparison to wt. All data are depicted as mean ± SEM; $N = 4$ isolations, $n = 500$ cells for both wt and *clic4*$^{-/-}$ cardiomyocytes; *$P < 0.05$, by one-way ANOVA test with Newman-Keuls post hoc analysis.

for $Ca^{2+}$ uptake by mitochondria at the ER-mitochondrial microdomains (*46*). Nevertheless, there is a possibility of posttranslational modification of MCU such as cysteine oxidation (*47*) or enhanced tyrosine phosphorylation (*48*) that is known to increase the activity of MCU. Earlier, it was shown that CsA does not rescue the reduced CRC arbitrated by the CLIC blocker IAA-94 (*8*). Our results indicate that CsA rescued the decreased CRC observed in *clic4*$^{-/-}$ cardiac mitochondria but not to a similar extent as wt. This suggests presence of either another target of IAA-94 in cardiac mitochondria which works in consortium with CLIC4 in regulating the effects of CsA or since *clic4*$^{-/-}$ cardiac mitochondria are already overloaded with $Ca^{2+}$, threshold levels are attained much earlier than wt.

In addition, our findings on caffeine-induced ER/SR to mitochondrial $Ca^{2+}$ transfer demonstrates that rapid release of $Ca^{2+}$ from SR upon RyR2 activation is accompanied by faster accumulation of $Ca^{2+}$ in mitochondria, suggesting a potential role for CLIC4 as a modulator of ER/SR-mitochondrial $Ca^{2+}$ transfer. We did not observe changes in cytoplasmic $Ca^{2+}$ transients recorded in the presence/absence of ISO in *clic4*$^{-/-}$ mouse adult cardiomyocytes in comparison to that of wt, thus suggesting that the absence of CLIC4 does not grossly affect the cytoplasmic $Ca^{2+}$ dynamics but probably increases the rate of $Ca^{2+}$ influx in the ER-mitochondrial domains under physiological conditions. Our study signifies the direct role of MAM-CLIC4 in maintaining ER/SR-mitochondrial $Ca^{2+}$ homeostasis.

Dysregulation of ER-mitochondrial communication is known to alter cardiac physiology and is very well implicated in IR injury to the heart (*49*). Previous studies also show that blocking $Cl^-$ channels with IAA-94 abrogates the cardioprotection mediated by ischemic/pharmacological preconditioning (*9*, *50*) and CsA (*51*) as well as causes early onset of mPTP opening (*8*). In this study, we demonstrate that *clic4*$^{-/-}$ mice hearts subjected to either in vivo or ex vivo IR injury assays showed enhanced MI and compromised left ventricular function in comparison to wt mice. Moreover, we observed a reduction in CRC in *clic4*$^{-/-}$ mice in comparison to cardiac mitochondria isolated from wt mice upon ex vivo IR injury. This suggests that increased $Ca^{2+}$ levels at the basal conditions in *clic4*$^{-/-}$ cardiomyocytes could possibly result in an early onset of mPTP opening upon stressful stimuli like IR injury. Similar to other reports (*8*, *9*, *50*), wt hearts preconditioned with IAA-94 showed increased MI, but no such changes were observed in *clic4*$^{-/-}$ hearts. In addition, in the presence of IAA-94, wt hearts showed infarction similar *to clic4*$^{-/-}$ hearts conditioned with vehicle control, ruling out the possibility of other CLICs in cardioprotection from IR injury. Thus, the cardio-deleterious effects of IAA-94 are mediated by targeting CLIC4. Earlier CLIC1 was shown to be present in intracellular organelles such as ER, lysosomes, and nucleus (*7*). In cardiomyocytes, CLIC1 is localized in ER (*19*); however, CLIC1 null mutant mice showed no difference in MI after IR injury, suggesting that the anionic gradient maintained by ER-CLIC1 does not affect cellular response to injury. Together, we can convincingly attribute the cardioprotective role to CLIC4 from IR injury by modulating mitochondrial physiology. In failing human hearts and mice hearts subjected to a chronic myocardial injury (8 weeks of LCA), enhanced expression of CLIC4 in cardiac sections was observed. We further subfractionated the cardiac tissue (*32*) and observed that CLIC4 expression in cytosol relative to organellar membrane fractions was enhanced in failing human hearts in comparison to healthy controls. Interestingly, CLIC1 did not show any difference in its distribution

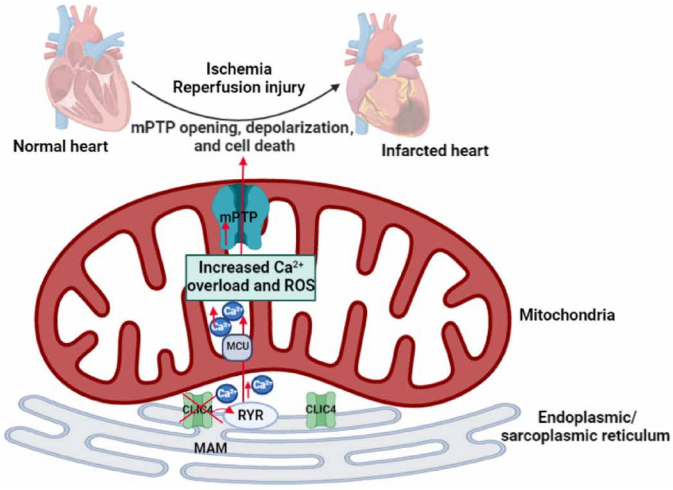


**Fig. 6. MAM-CLIC4 is important for ER-mitochondrial $Ca^{2+}$ homeostasis and plays a key role in cardioprotection from IR injury by modulating mitochondrial function.**

in HF cardiac tissue. The lesser extent of internalization of soluble CLIC4 to the organelle membrane in failing heart may contribute to its decreased functional activity in intracellular membrane fraction like MAM and potentially result in the pathological consequences during HF. Thus, the mechanism of changes in the distribution of CLIC4 in subcellular fractions during HF needs to be elucidated for complete understanding of its role.

Inhibition of CLIC4 is known to induce apoptosis in human head and neck squamous carcinoma cell line (HN4) by causing mitochondrial membrane depolarization (*52*). Here, we found that *clic4*$^{-/-}$ cardiomyocytes subjected to HR injury showed increased apoptosis and mitochondrial membrane depolarization in comparison to wt cardiomyocytes. Both increases in $Ca^{2+}$ overload and ROS production are known to induce the formation and opening of mPTP leading to cell death (*53*). Upon HR injury, *clic4*$^{-/-}$ cardiomyocytes showed increased ROS production relative to wt cardiomyocytes, suggesting that, in addition to increased $Ca^{2+}$ overload observed in *clic4*$^{-/-}$ mice hearts, elevated ROS production during reperfusion could be responsible for the mitochondrial membrane depolarization and cell death. Our results establish the direct role of MAM-CLIC4 in cardiomyocytes in cellular protection from HR injury.

To recapitulate, our results present a novel $Cl^-$ channel, CLIC4, in MAM that plays a fundamental role in regulating ER/SR-mitochondrial $Ca^{2+}$ homeostasis (Fig. 6). Furthermore, our results highlight the unprecedented role of MAM-CLIC4 in regulating myocardial injury and cardiac function after hypoxia/IR injury by regulating mitochondrial membrane potential and oxidative stress (Fig. 6). Thus, we speculate that the role of MAM-CLIC4 in mediating ER-mitochondrial communication would also affect other physiological and pathophysiological processes.

## MATERIALS AND METHODS

All procedures carried on mice are according to the National Institutes of Health *Guide for the Care and Use of Laboratory Animals* and approved by the Ohio State University committee on animal care. All experiments on the human heart were conducted under

the approval of the Institutional Review Board of The Ohio State University. The published data, methods, and null mutant mice will be made available to other researchers for the purpose of reproducing results or replicating the procedure.

### Cell lines

HEK 293T cells were cultured in Dulbecco's modified Eagle's medium (DMEM) containing 1× GlutaMAX, glucose (4.5 g/liter), 1 mM sodium pyruvate, sodium bicarbonate (1.5 g/liter), 10% (v/v) fetal bovine serum (FBS), and penicillin (100 IU)/streptomycin (100 μg/ml). The cells were incubated in humidified 5% (v/v) $CO_2$ incubators at 37°C and passaged once every 3 days.

### Cloning

Truncated *clic4* clones were generated using site directed mutagenesis by "Quick change" method. We used *pCDNA3.1-clic4* encoding N-terminal FLAG as a template. Briefly, sense and antisense primers (table S1) carrying the site-specific mutation to introduce a stop codon at glutamine-67 and cysteine-189 were used to amplify the constructs *CLIC4ΔQ67* and *CLIC4ΔC189*, respectively. The reaction mixture was prepared according to the manufacturer's protocol containing 200 ng of *pcDNA3.1 CLIC4* plasmid for 20 amplification cycles. The amplification reaction mixture was digested with the *Dpn1* enzyme overnight at 37°C. DH5α competent cells were transformed with the reaction mixture by heat shock and plated on LB agar plates containing ampicillin (100 μg/ml) at 37°C for 12 hours. The positive colonies were screened by Sanger sequencing.

### HEK cell transfection

HEK cells were seeded at a density of 15,000 cells on a glass coverslip (0.13 mm thickness) coated with poly-D-lysine and cultured overnight. Once the cells reached 70% confluency, they were transfected with 200 ng of Flag-tagged *pCDNA-CLIC4, pCDNA-CLIC4ΔQ67*, and *pCDNA-CLIC4ΔC189*, respectively, using Lipofectamine 2000 per the manufacturer's instructions (Thermo Fisher Scientific). After 16 hours of transfection, the cells were loaded with 200 nM MitoTracker at 37°C for 10 min, washed, and processed for immunocytochemistry.

### Isolation of mouse adult/neonatal cardiomyocytes and crude mitochondria

#### *Adult cardiomyocytes*

Mouse adult cardiomyocytes were isolated using the simplified Langendorff-free method of isolation (*54*) from wt and *clic4*$^{-/-}$ mice. Briefly, mice were anesthetized, and the chest was opened to expose the heart. The descending aorta was cut, followed by an injection of 7 ml of EDTA buffer [130 mM NaCl, 5 mM KCl, 0.5 mM $NaH_2PO_4$, 10 mM Hepes, 10 mM glucose, 10 mM butanedione monoxime (BDM), 10 mM taurine, and 5 mM EDTA (pH 7.8)] into the right ventricle. The ascending aorta was clamped, and the heart was transferred to a petri dish containing EDTA buffer. The left ventricle was injected with 10 ml of EDTA buffer, followed by 3 ml of perfusion buffer [130 mM NaCl, 5 mM KCl, 0.5 mM $NaH_2PO_4$, 10 mM Hepes, 10 mM glucose, 10 mM BDM, 10 mM taurine, and 1 mM $MgCl_2$ (pH 7.8)], and 30 ml of collagenase enzyme solution [collagenase 2 (0.5 mg/ml), collagenase 4 (0.5 mg/ml), and protease XIV prepared in perfusion buffer (0.05 mg/ml)]. The heart chambers were separated and gently pulled into 1-mm pieces. The cells were dissociated using gentle trituration, and the collagenase activity was inhibited by 5 ml of stop buffer [perfusion buffer containing 5% (v/v) sterile FBS]. The cells were washed three times with perfusion buffer and allowed to settle with gravity. The cardiomyocytes were then loaded with 200 nM MitoTracker at 4°C for 1 hour. The MitoTracker- loaded cardiomyocytes were then spread on a poly-L-lysine–treated coverslip for 1 hour and processed for immunocytochemistry.

#### *Mouse neonatal cardiomyocytes*

MNCMs were isolated as described previously (*19*, *55*) from wt and *clic4*$^{-/-}$ mice. Briefly, hearts were surgically excised from p3 pups from wt mice and placed in a dissociation buffer [16 mM NaCl, 20 mM Hepes, 0.8 mM $Na_2HPO_4$, 5.4 mM glucose, 5.4 mM KCl, and 0.8 mM $MgSO_4$ (pH 7.35)]. Ventricles were minced in dissociation buffer, followed by centrifugation at 1000*g* for 5 min at 4°C. The tissue pellet was resuspended in a dissociation buffer containing 0.25% trypsin and incubated at 37°C for 20 min in the water bath shaker for digestion. After 20 min, the cells were spun down (1000*g*, 5 min, 4°C), and the dissociated neonatal cardiomyocytes in the supernatant were collected by passing through a cell strainer (100 μm) and immediately enriched with 20% (v/v) horse serum. The digestion of the remaining tissue pellet was repeated at least twice or until a clear tissue pellet was observed. The dissociated neonatal cardiomyocytes were then seeded on gelatin [0.1% (w/v)]–coated coverslips and cultured in DMEM containing 20% (v/v) FBS and penicillin (100 IU)/streptomycin (100 μg/ml), in humidified 5% (v/v) $CO_2$ incubators at 37°C, and the medium was changed after 2 days. After the fourth day of isolation, the MNCMs were loaded with 200 nM MitoTracker at 37°C for 10 min, washed with phosphate-buffered saline (PBS), and processed for immunolabeling.

#### *Crude mitochondria*

*Wt*, *clic1*$^{-/-}$, and *clic4*$^{-/-}$ mice (12 to 15 weeks) hearts were isolated and finely minced and homogenized in isolation buffer A [70 mM sucrose, 210 mM mannitol, 10 mM EDTA-$Na_2$, and 50 mM tris-HCl (pH 7.4)] using a Potter-Elvehjem homogenizer (seven strokes). The homogenate was centrifuged at 1300*g* for 5 min at 4°C. The supernatant was transferred into a fresh Eppendorf tube and centrifuged at 10,000*g* for 10 min at 4°C. The pellet containing crude mitochondria was resuspended in isolation buffer A containing 200 nM MitoTracker and incubated at 4°C for 1 hour. The MitoTracker-loaded mitochondria were spread on a poly-L-lysine–treated coverslip for 1 hour at 4°C. The mitochondria were then processed for immunolabeling.

### Isolation of ultrapure mitochondria

Ultrapure mitochondrial fractions were isolated as described earlier (*11*). Briefly, a mouse heart (12 to 15 weeks) after homogenization in isolation buffer A (70 mM sucrose, 210 mM mannitol, 10 mM EDTA-$Na_2$, and 50 mM tris-HCl (pH 7.4)] was centrifuged at 1300*g* for 5 min at 4°C. The supernatant was centrifuged again at 10,000*g* for 10 min at 4°C. The pellet containing crude mitochondria was resuspended in 55 μl of isolation buffer A. The resuspended crude mitochondrial preparation was overlaid on 3 ml of 30% (v/v) Percoll prepared in buffer B (250 mM sucrose, 10 mM Hepes-Na, and 1 mM EDTA-$Na_2$ (pH 7.4)]. The sample was centrifuged at 50,000*g* for 45 min at 4°C. After ultracentrifugation, three clear layers were obtained, which were labeled as M1, M2, and M3, where M3 is the ultrapure mitochondrial fraction. M1, M2, and M3 layers were carefully isolated, resuspended in 1 ml of buffer A, and centrifuged at 12,000*g* for 10 min (three times) at 4°C. The pellet was resuspended

in radioimmunoprecipitation assay (RIPA) buffer [50 mM tris-HCl, 150 mM NaCl, 1 mM EDTA-$Na_2$, 1 mM EGTA-$Na_4$, 1% (v/v) NP-40, 0.5% (w/v) Na-deoxycholate, 0.1% (w/v) SDS, 1 mM NaF, 1 mM phenylmethylsulfonyl fluoride, and 1 mM $Na_3VO_4$ (pH 7.4) containing protease inhibitors (1 tablet/50 ml, Roche) and phosphatase inhibitor (1 tablet/10 ml, Roche)], frozen in liquid nitrogen, and processed for Western blot analysis.

### Isolation of MAMs and mitochondria

MAM fractions were isolated as published earlier (*10*, *56*). Briefly, mouse hearts (12 to 15 weeks) were isolated, minced, and homogenized in buffer IB-H1 [225 mM mannitol, 75 mM sucrose, 0.5% (w/v) bovine serum albumin (BSA), 0.5 mM EGTA, and 30 mM tris-HCl (pH 7.4)] using a Potter-Elvehjem homogenizer (eight strokes). The homogenate was centrifuged twice at 740*g* for 5 min each at 4°C. The supernatant was collected and centrifuged again at 9000*g* for 10 min at 4°C. The supernatant was removed (cytosol), and the pellet was gently resuspended in ice-cold buffer IB-H2 [225 mM mannitol, 75 mM sucrose, 0.5% (w/v) BSA, and 30 mM tris-HCl (pH 7.4)] and centrifuged at 10,000*g* for 10 min at 4°C. The supernatant was discarded, and the pellet was resuspended in buffer IB-H3 [225 mM mannitol, 75 mM sucrose, and 30 mM tris-HCl (pH 7.4)] and centrifuged again at 10,000*g* for 10 min at 4°C. The pellet containing crude mitochondria was resuspended in 55 μl of mitochondria resuspending buffer (MRB) [250 mM mannitol, 0. mM 5 EGTA, and 5 mM Hepes (pH 7.4)]. The crude mitochondrial pellet was overlaid on 3 ml of 30% (v/v) Percoll prepared in Percoll medium [225 mM mannitol, 1 mM EGTA, and 25 mM Hepes (pH 7.4)] and centrifuged at 95,000*g* for 30 min at 4°C. This step separates the MAM (upper band) and mitochondria (lower band). The lower band containing mitochondria was collected and resuspended in MRB buffer and centrifuged at 10,000*g* for 10 min at 4°C. The pellet obtained after centrifugation was resuspended in RIPA buffer and frozen in liquid nitrogen. The upper band containing MAM was diluted in MRB buffer and further centrifuged at 10,000*g* for 10 min at 4°C. The supernatant was collected and centrifuged at 100,000*g* for 1.5 hours at 4°C. The MAM pellet was collected, resuspended in RIPA buffer, and frozen in liquid nitrogen. All the cellular fractions including crude heart lysates, cytosol, crude mitochondria, purified mitochondrial, and MAM fractions were subjected to three repeated freeze-thaw cycles and processed for Western blot analysis.

### G-CEPIA1er imaging

MNCMs were infected and cultured with G-CEPIA1er virus (*15*) on glass coverslips. After 48 to 72 hours, CMs were perfused with Tyrode's solution containing 2 mM $Ca^{2+}$. Biosensor G-CEPIA1er was excited using a 488-nm line of an Ar laser, and fluorescence emission was collected at 500 to 550 nm, measured in *x-y* mode at 400-Hz sampling rate. Myocytes were exposed to SERCa2a inhibitor thapsigargin (10 μM) after 2 min, and the fluorescence signal was monitored using confocal microscopy. The time constant of decay of G-CEPIA1er was used as a measure of SR leak, fitting fluorescence data to a monoexponential function (*57*). The SR $Ca^{2+}$ store was depleted by the application of high-dose caffeine (10 mM) in $Ca^{2+}$-free Tyrode's solution.

### mtRCamp1h imaging

To assess mito-$Ca^{2+}$ handling, MNCMs were infected with mtRCamp1h virus (*16*) on glass coverslips and cultured for 48 to 72 hours. Biosensor mtRCamp1h was excited using a 543-nm line of HeNe laser, and fluorescence emission was collected at 560- to 660-nm wavelengths, measured in the *x-y* mode and 400-Hz sampling rate. Myocytes were perfused with Tyrode's solution (2 mM $Ca^{2+}$). A subgroup of *clic4*$^{-/-}$ MNCMs was preincubated with Ru360 (1 μM) for 10 min before recording. After 5 min of recording, CMs were washed in $Ca^{2+}$-free Tyrode's solution before permeabilization with saponin [0.001% (v/v)]. The solution was replaced with an internal recording solution containing cytochalasin D (10 μM) and $Ca^{2+}$ buffer EGTA (2 mM) to obtain minimum mtRCamp1h fluorescence. Maximum fluorescence was achieved by application of $Ca^{2+}$ (20 μM). Using the equation

$$[Ca^{2+}]_m = K_d \times (F - F_{min})/(F_{max} - F)$$

where dissociation constant ($K_d$) of mtRCamp1h = 1.3 μM, fluorescence was converted to $[Ca^{2+}]_m$ for each MNCM.

### Cytosolic and mitochondrial $Ca^{2+}$ in neonatal mouse cardiomyocytes

MNCMs were infected with mtRCamp1h virus on glass coverslips (*16*). After 48 to 72 hours, infected MNCMs were also loaded with Fluo-3 AM (Invitrogen) at room temperature (RT) for 10 min in Tyrode's solution containing 2 mM $Ca^{2+}$, followed by a 10-min wash in Tyrode's solution containing 2 mM $Ca^{2+}$. Myocytes were perfused with Tyrode's solution containing 2 mM $Ca^{2+}$ at RT during recordings. Biosensor mtRCamp1h was excited using a 543-nm line of HeNe laser and fluorescence emission was collected at 560- to 660-nm wavelengths, and Fluo-3 AM was excited at 488 nm and fluorescence emission was collected at 500- to 530-nm wavelengths, in linescan mode. Caffeine was applied at 10 mM to induce RyR2-mediated $Ca^{2+}$ release. $Ca^{2+}$ transient amplitudes are presented as $\Delta F/F_0$, where $F_0$ is basal fluorescence and $\Delta F = F - F_0$.

### $Ca^{2+}$ imaging of adult mouse cardiomyocytes

Confocal imaging of cytosolic $Ca^{2+}$ was performed as described previously (*17*) . Briefly, fresh adult mouse cardiomyocytes (*54*) were loaded with Fluo-3 AM (Invitrogen) at RT for 10 min in Tyrode's solution containing 1 mM $Ca^{2+}$, followed by a 10-min wash in Tyrode's solution containing 2 mM $Ca^{2+}$. Myocytes were perfused with Tyrode's solution containing 2 mM $Ca^{2+}$ at RT during recordings. Fluo-3 AM was excited at 488 nm, and fluorescence emission was collected at 500- to 530-nm wavelengths, in linescan mode at 200 Hz. Myocytes were paced at 0.5 Hz. β-Adrenergic agonist ISO was used at 100 nM. Caffeine was applied at 10 mM at the end of the experiment to assess SR $Ca^{2+}$ content. Cytosolic $Ca^{2+}$ transient amplitude and caffeine transient amplitude are presented as $\Delta F/F_0$, where $F_0$ is basal fluorescence and $\Delta F = F - F_0$. SERCa2a rate was calculated by fitting a single exponential to the caffeine-induced $Ca^{2+}$ transient and then fitting a two-component exponential to the cytosolic $Ca^{2+}$ transient with a fixed first tau.

### Fura-2AM staining of cardiomyocytes

Briefly, freshly isolated cardiomyocytes after reintroduction with $Ca^{2+}$ (*54*) were resuspended in in myocyte culture medium [M199 with 5% BSA, BDM (1 mol/ml), and 1× penicillin/streptomycin]. For calcium measurements, the adult cardiomyocytes were loaded with Fura-2AM (0.5 μM) (*20*) for 20 min before data collection. Data were collected using an IonOptix system (IonOptix) connected to a Motic AE31 microscope, visualized on a 40× objective, and

stimulated with 20 V at 1 Hz. Changes in intracellular $Ca^{2+}$ levels were monitored using Fura-2 dual-excitation (340/380 nm) single-emission (510 nm) ratiometric imaging. Measurements were taken at baseline and upon ISO treatment (100 nM).

### Langendorff perfusion of heart for performing ex vivo IR injury

Wt CD1 and *clic4*$^{-/-}$ mice (12 to 15 weeks) obtained from in-house breeding were Langendorff-perfused as described previously (*12*). Briefly, hearts were excised from the mice and placed in ice-cold Krebs-Henseleit buffer (KHB) (118 mM NaCl, 4.7 mM KCl, 1.2 mM $KH_2PO_4$, 1.2 mM $MgSO_4$, 25 mM $NaHCO_3$, 11.1 mM D-glucose, and 2 mM $CaCl_2$). The aorta was cannulated, and the heart was perfused in a retrograde manner on a Langendorff apparatus with KHB bubbled with 95% $O_2$–5% $CO_2$. The heart was perfused for 15 min, followed by ischemia for 25 min and reperfusion for 2 hours at 37°C. For sham control, the heart was continuously perfused for 160 min at 37°C. In certain cases, the heart was postconditioned with either DMSO (vehicle control) or IAA-94 (50 μM) for 10 min before reperfusion. For assessing CRC, the hearts were subjected to 25 min of ischemia and reperfused for 20 min. After reperfusion, the hearts were either processed to assess mitochondrial CRC or stained with TTC to assess infarct size.

### In vivo IR injury and permanent ligation

IR injury was performed in mice both using the classical method and the new method of induction of myocardial IR injury as described previously (*23*). The LCA was ligated for 40 min, followed by reperfusion for 24 hours. The surgeries were performed within 2 min when the ventilator was not used. Briefly, a small skin cut was made over the left chest, and a purse suture was made. After dissection, the pectoralis minor muscle was retracted to expose the fourth intercostal space. A small incision was made at the fourth intercostal space, and the heart was "popped out" gently. The left descending coronary artery was sutured, and a slipknot was tied around the LCA 2 to 3 mm from its origin using a 6-0 silk suture. After ligation, the heart was placed back into the intrathoracic space, and the air was removed manually before the closure of muscle and skin. The internal needle end of the slipknot is cut short, and the other end of the suture remains outside the chest and is 0.8 cm long. After 40 min of ischemia, the slipknot is released by pulling the long end of the suture gently and smoothly to cause reperfusion in the heart. For the classical method of in vivo IR injury, the mice were anesthetized with 3% (v/v) isoflurane and intubated with a 20-gauge intravenous catheter and ventilated with $O_2$ and 2% (v/v) isoflurane. After dissection, the coronary artery was sutured in a similar manner as the nonclassical method of IR injury. The mice were ventilated continuously during the 40 min of ischemia, and the incision was covered with saline-soaked gauze. After the ischemic period, the slipknot was released followed by closing the chest. The sham group underwent the same surgery but without occlusion of the LCA. The echocardiography imaging of mice was performed at the basal level and also after 24 hours of reperfusion. For chronic myocardial ischemic injury, the hearts were not reperfused but were continuously ligated for 8 weeks.

### Evans blue/TTC staining

In the case of in vivo IR injury, after 24 hours of reperfusion, the mice were anesthetized, the chest was opened, and the ligature around the LCA was retied through the previous ligation. A total of 20 μl of 2% (w/v) Evans blue dye was injected through the aorta. The heart is quickly excised, frozen, and sliced into thick sections that are perpendicular to the long axis of the heart. The unstained portion is defined as an AAR. The sections were then incubated with 1% TTC (prepared in PBS) at RT for 15 min, fixed with 4% (w/v) paraformaldehyde (PFA) for 5 min, and imaged using Leica S9i. The myocardial infarct size (pale) is quantified using ImageJ and expressed as a percentage of infarct area over AAR. AAR is calculated as a percentage of AAR over the total area of the left ventricle. The hearts from ex vivo IR injury were also frozen and stained with TTC, and the infarct size was calculated.

### Echocardiography imaging

A high-frequency, high-resolution ultrasound imaging system was used for echocardiography (Vevo 2100 and Vevo 3100 Imaging System, FUJIFILM VisualSonics Inc., Toronto, Canada). For cardiovascular function assessment of wt and *clic4*$^{-/-}$ mice, a high-frequency transducer probe (VisualSonics MS400 with a frequency range of 18 to 38 MHz and VisualSonics MX550D with a frequency range of 25 to 55 MHz, FUJIFILM VisualSonics Inc., Toronto, Canada) was used. Briefly, mice were anesthetized with 1.5 to 2% (v/v) isoflurane mixed with $O_2$, and the heart rate was maintained between 400 and 450 beats per minute. M and B mode images were acquired along the parasternal long-axis view to measure cardiac function. Images were analyzed using Vevo LAB 3.1.1 analysis software.

### Western blot analysis

Different cellular fractions obtained during MAM and ultrapure mitochondrial preparation that were resuspended in RIPA buffer were incubated for 1 hour at 4°C with continuous shaking. The whole hearts from wt and *clic4*$^{-/-}$ mice or cardiac section from the border zone region after IR injury was minced in RIPA buffer and homogenized to prepare heart lysates. The lysates were snap-frozen in liquid nitrogen and, once thawed, were incubated at 4°C with continuous shaking for 1 hour. After 1 hour, samples were centrifuged at 12,000*g* for 20 min at 4°C, the supernatant was collected and loaded on 4 to 20% (w/v) SDS–polyacrylamide gel electrophoresis and transferred to nitrocellulose membranes. Protein loading was corroborated with Ponceau S staining. Membranes were blocked with a LI-COR blocking buffer and washed with tris-buffered saline (TBS) before incubating overnight with various primary antibodies at 4°C. Primary antibodies used were GRP78/BIP (ab21685), CLIC4 (sc-135739), CLIC1 (sc-374202), adenosine triphosphate (ATP) synthase (ab14748), MCU (14997), glyceraldehyde-3-phosphate dehydrogenase (GAPDH) (2118), mitofusin 2 (ab-205236), ACSL4 (PA5-27137), prohibitin (ab-10198), cytochrome c (pa1-12250), and cyclophilin D (AP1035). After washing thrice with TTBS (20 mM Tris buffer saline containing 0.05% Tween-20) for 10 min each, membranes were incubated with anti-rabbit/mouse secondary antibodies conjugated to IR680/IR800 for 1 hour at RT and washed again thrice with TTBS for 5 min. Signals were visualized using an infrared fluorescence system (Bio-Rad). The intensity of the bands was quantified using ImageJ and normalized to loaded protein using Ponceau S signals for different subcellular fractions. In certain cases, the protein amount was normalized to the respective GAPDH control.

### HR injury

Neonatal cardiomyocytes were subjected to 6 hours of hypoxia and 12 hours of reoxygenation injury. After 4 days of culturing the neonatal

cardiomyocytes in 35-mm glass-bottom petri dishes or coverslips coated with 0.1% (w/v) gelatin, cells were subjected to hypoxia in a modular humidified 37°C hypoxia chamber (Biospherix, C127) with 1% (v/v) $O_2$, 5% (v/v) $CO_2$, and balanced $N_2$ for 6 hours in DMEM containing no glucose and FBS. After hypoxia, the cells are reperfused in DMEM containing glucose (4 g/liter) and 20% (v/v) FBS and cultured for 12 hours. The cells after reperfusion are processed for JC1 staining to assess membrane potential, 2′,7′-Dichlorodihydrofluorescein diacetate (DCFDA) for ROS measurements, and TUNEL assay for assessing cell death. Image analysis was done using ImageJ.

### Immunolabeling

Isolated crude mitochondria, adult, or neonatal cardiomyocytes, HEK-transfected cells, and neonatal cardiomyocytes subjected to normoxia/HR injury were loaded with MitoTracker as described in the previous section, followed by fixing with 4% (w/v) PFA for 10 min at RT (*12*). Next, the crude mitochondria, cardiomyocytes, and HEK cells were permeabilized with 0.5% (v/v) Triton X-100 for 10 min at RT, followed by blocking with 10% normal goat serum (NGS) for 30 min at RT. The samples were then incubated with the various specific primary antibodies [diluted in PBS containing 1% (w/v) NGS and 0.1% (v/v) Triton X-100] at 4°C overnight. After incubation with the primary antibodies, GRP78/BIP (ab21685), CLIC4 (sc-135739), CLIC1 (sc-374202), ATP synthase (ab14748), mitofusin 2 (ab-205236), ACSL4 (PA5–27137), prohibitin (ab-10198), and cytochrome c (pa1-12250), the samples were washed (three times) with PBS containing 0.1% (v/v) Triton X-100 and incubated with secondary antibodies conjugated to anti-mouse/rabbit Alexa Fluor 488 (2 μg/ml) and anti-rabbit/mouse Atto 647N (1 μg/ml) for 1 hour at RT. The samples were stained with 4′,6-diamidino-2-phenylindole dihydrochloride (DAPI) (nuclei marker; 1:10,000) and mounted with either Mowiol 4-88 or Prolong Gold (Molecular Probes). Cells were imaged with a Nikon A1R high-resolution confocal microscope and median-filtered (*8*). The percentage colocalization index was calculated using ImageJ.

### ROS measurement

ROS production was measured using Chloromethyl 22′,7′-Dichlorodihydrofluorescein diacetate (CM-H2DCFDA) (Life Technologies, C26827). Neonatal cardiomyocytes following reperfusion were stained with DCFDA (10 μM) in regular DMEM without phenol red for 30 min. After staining, the cells were washed with DMEM without phenol red and imaged in the same medium using a Nikon A1R confocal microscope at excitation and emission wavelengths of 485/535 nm. Cells in normoxia are used as controls and are processed similarly. The fluorescence intensities were quantified using ImageJ. The fold change in ROS production relative to normoxia is represented in bar graph.

### TUNEL assay

The neonatal cardiomyocytes after HR injury or upon normoxia (control) were fixed with 4% (w/v) PFA for 10 min, permeabilized with 0.25% (v/v) Triton X-100 for 20 min, and stained with TUNEL using a TUNEL assay kit per the manufacturer's instructions (Thermo Fisher Scientific). The cells were counterstained with DAPI to stain for the nucleus. Fluorescent images were obtained using a Nikon A1R confocal microscope with the excitation-emission wavelength of 488 and 530 nm, respectively.

### Calcium retention capacity

Hearts from wt and *clic4*$^{-/-}$ mice were washed in PBS, minced, and homogenized in buffer A [70 mM sucrose, 210 mM mannitol, 1 mM EDTA, and 50 mM tris HCl (pH 7.4)] using a Potter Elvehjem homogenizer (seven strokes). The homogenate was centrifuged at 2500*g* for 5 min. The supernatant was collected and centrifuged at 12,000*g* for 10 min. The pellet containing crude mitochondria was resuspended in 55 μl of buffer B [70 mM sucrose, 210 mM mannitol, 0.1 mM EDTA, and 50 mM tris-HCl (pH 7.4)]. Extramitochondrial calcium was detected by Calcium Green using a fluorescence spectrophotometer (Hitachi F-2710 or Hitachi F-7100). Calcium Green-5N, Hexapotassium Salt (2.5 μM) (Thermo Fisher Scientific, 10 μl from 500 μM stock) was added in certain groups in the presence and absence of CsA to the CRC buffer [150 mM sucrose, 50 mM KCl, 2 mM $KH_2PO_4$, 5 mM succinic acid, and 20 mM tris-HCl (pH 7.4)] at 25°C, and the fluorescence was measured (excitation at 500 nm and emission at 530 nm). After 30 s, 50 μl of isolated mitochondria sample was added. After another 90 s and subsequently at every 60 s thereafter, 5 μM $CaCl_2$ pulses were added until a rapid increase in fluorescence indicated mitochondrial death. The protein estimation was performed for the mitochondria using a Bio-Rad kit according to the manufacturer's instructions. The fluorescence values were normalized with respect to the protein concentration, and the calcium required to induce mitochondrial death is compared between the different experimental groups.

### JC1 staining to assess mitochondrial membrane potential loss

Neonatal cardiomyocytes under normoxia and HR injury conditions were stained with JC1 dye (*33*) for 30 min at 37°C in a humidified 5% (v/v) $CO_2$ incubator. The cells were then washed with DMEM without phenol red and imaged using a Nikon A1R confocal microscope. JC1 dye is an indicator of mitochondrial membrane potential. At higher mitochondrial membrane potential, JC1 dye accumulates in the mitochondria and forms red J1 aggregates that emit at 590 nm. At lower membrane potential, JC1 dye remains in the green monomeric form and emits at 530 nm. The ratio of fluorescence intensities of red versus green defines the changes in mitochondrial membrane potential change.

### Immunohistochemistry of mouse and human heart sections

Both human and mouse tissue sections were deparaffinized in xylene and rehydrated with ethanol and PBS, followed by antigen retrieval using citrate-based buffer (Vector Laboratories, #H-3300-250). Failing human cardiac tissues were obtained with Institutional Review Board approval and informed consent, and the non-failing cardiac tissue was procured in collaboration with the Lifeline of Ohio Organ Procurement program. Sections were incubated at RT with 3% (v/v) $H_2O_2$ for 10 min to quench endogenous peroxidase activity and blocked by 5% (w/v) NGS in PBS for 1 hour. After blocking, sections were incubated with wheat germ agglutinin (WGA) (1:500 of 1 mg/ml for 60 min at RT to the label plasma membrane. After WGA staining, sections were washed with PBS three times 5 min each. Sections were incubated with 0.5% (v/v) Triton X-100 containing PBS for 10 min at RT for permeabilization. After three washes with PBS, sections were incubated with anti-CLIC4, anti-prohibitin, and anti–cytochrome c antibody at 4°C overnight. After primary antibody incubation, sections were washed with 0.1% (v/v) Triton X-100 containing PBS and then incubated with secondary antibodies. After secondary antibody incubation, sections were washed and stained

with DAPI (1:10,000 dilution) followed by mounting with either Mowiol 4-88 or Prolong Gold (Molecular Probes). Cells were imaged with a Nikon A1R high-resolution confocal microscope and median-filtered (*8*).

### Subfraction of human cardiac tissue

Frozen human cardiac tissues were subfractionated as described previously (*32*). Briefly, 150 mg of tissue was homogenized in cell lysis buffer (CLB) buffer [10 mM Hepes, 10 mM NaCl, 1 mM $KH_2PO_4$, 5 mM $NaHCO_3$, 5 mM EDTA, 1 mM $CaCl_2$, 0.5 mM $MgCl_2$ (pH 7.5), and complete protease inhibitor tablet], and isotonicity was restored by adding 100 µl of 2.5 M sucrose. Homogenate was centrifuged at 6300*g* for 10 min at 4°C. The supernatant was transferred into a fresh tube (sup1), and the pellet was resuspended in 500 µl of CLB/0.25 M sucrose and recentrifuged at 6300*g* for 5 min at 4°C. The supernatant (sup2) was pooled with the previous sample of supernatant (sup1), and the pellet was resuspended in 1 ml of TSE buffer [10 mM tris, 300 mM sucrose, 1 mM EDTA, and 0.1% (v/v) NP-40 (pH 7.5)] and homogenized (30 strokes). The sample was centrifuged at 4000*g* for 5 min at 4°C. The final pellet obtained after homogenization with TSE buffer is resuspended in RIPA buffer and represents an enriched nuclear fraction. The pooled supernatant (sup1 and sup2) was centrifuged at 107,000*g* for 30 min at 4°C in a Beckman ultracentrifuge. The supernatant obtained after the centrifugation step represents the cytosolic fraction. The pellet obtained after ultracentrifugation is resuspended in RIPA buffer and represents the membrane and organellar fraction. The lysates were processed for Western blotting and probed with anti-CLIC1 and anti-CLIC4 antibodies. The expression of CLIC4 and CLIC1 was normalized to total protein content detected by Ponceau S staining of the blot by quantifying the band intensities using ImageJ software analysis.

## SUPPLEMENTARY MATERIALS

Supplementary material for this article is available at https://science.org/doi/10.1126/sciadv.abo1244

## REFERENCES AND NOTES


1. C. Giorgi, S. Missiroli, S. Patergnani, J. Duszynski, M. R. Wieckowski, P. Pinton, Mitochondria-associated membranes: Composition, molecular mechanisms, and physiopathological implications. *Antioxid. Redox Signal.* **22**, 995–1019 (2015).
2. S. Missiroli, S. Patergnani, N. Caroccia, G. Pedriali, M. Perrone, M. Previati, M. R. Wieckowski, C. Giorgi, Mitochondria-associated membranes (MAMs) and inflammation. *Cell Death Dis.* **9**, 329 (2018).
3. D. L. Lewis, J. D. Lechleiter, D. Kim, C. Nanavati, D. E. Clapham, Intracellular regulation of ion channels in cell membranes. *Mayo Clin. Proc.* **65**, 1127–1143 (1990).
4. C. N. Poston, S. C. Krishnan, C. R. Bazemore-Walker, In-depth proteomic analysis of mammalian mitochondria-associated membranes (MAM). *J. Proteomics* **79**, 219–230 (2013).
5. E. Argenzio, W. H. Moolenaar, Emerging biological roles of $Cl^-$ intracellular channel proteins. *J. Cell Sci.* **129**, 4165–4174 (2016).
6. S. G. Rao, N. J. Patel, H. Singh, Intracellular chloride channels: Novel biomarkers in diseases. *Front. Physiol.* **11**, 96 (2020).
7. S. G. Rao, D. Ponnalagu, N. J. Patel, H. Singh, Three decades of chloride intracellular channel proteins: From organelle to organ physiology. *Curr. Protoc. Pharmacol.* **80**, 11.21.1–11.21.17 (2018).
8. D. Ponnalagu, A. T. Hussain, R. Thanawala, J. Meka, P. Bednarczyk, Y. Feng, A. Szewczyk, S. Gururaja Rao, J. C. Bopassa, M. Khan, H. Singh, Chloride channel blocker IAA-94 increases myocardial infarction by reducing calcium retention capacity of the cardiac mitochondria. *Life Sci.* **235**, 116841 (2019).
9. R. J. Diaz, V. A. Losito, G. D. Mao, M. K. Ford, P. H. Backx, G. J. Wilson, Chloride channel inhibition blocks the protection of ischemic preconditioning and hypo-osmotic stress in rabbit ventricular myocardium. *Circ. Res.* **84**, 763–775 (1999).
10. M. R. Wieckowski, C. Giorgi, M. Lebiedzinska, J. Duszynski, P. Pinton, Isolation of mitochondria-associated membranes and mitochondria from animal tissues and cells. *Nat. Protoc.* **4**, 1582–1590 (2009).
11. H. Singh, R. Lu, P. F. G. Rodríguez, Y. Wu, J. C. Bopassa, E. Stefani, L. Toro, Visualization and quantification of cardiac mitochondrial protein clusters with STED microscopy. *Mitochondrion* **12**, 230–236 (2012).
12. H. Singh, R. Lu, J. C. Bopassa, A. L. Meredith, E. Stefani, L. Toro, mitoBK$_{Ca}$ is encoded by the *Kcnma1* gene, and a splicing sequence defines its mitochondrial location. *Proc. Natl. Acad. Sci. U.S.A.* **110**, 10836–10841 (2013).
13. H. Singh, R. H. Ashley, CLIC4 (p64H1) and its putative transmembrane domain form poorly selective, redox-regulated ion channels. *Mol. Membr. Biol.* **24**, 41–52 (2007).
14. C. García-Pérez, G. Hajnóczky, G. Csordás, Physical coupling supports the local $Ca^{2+}$ transfer between sarcoplasmic reticulum subdomains and the mitochondria in heart muscle. *J. Biol. Chem.* **283**, 32771–32780 (2008).
15. S. Hamilton, R. Terentyeva, B. Martin, F. Perger, J. Li, A. Stepanov, I. M. Bonilla, B. C. Knollmann, P. B. Radwański, S. Györke, A. E. Belevych, D. Terentyev, Increased RyR2 activity is exacerbated by calcium leak-induced mitochondrial ROS. *Basic Res. Cardiol.* **115**, 38 (2020).
16. S. Hamilton, R. Terentyeva, T. Y. Kim, P. Bronk, R. T. Clements, J. O-Uchi, G. Csordás, B. R. Choi, D. Terentyev, Pharmacological modulation of mitochondrial $Ca^{2+}$ content regulates sarcoplasmic reticulum $Ca^{2+}$ release via oxidation of the ryanodine receptor by mitochondria-derived reactive oxygen species. *Front. Physiol.* **9**, 1831 (2018).
17. S. Hamilton, R. Terentyeva, F. Perger, B. H. Orengo, B. Martin, M. W. Gorr, A. E. Belevych, R. T. Clements, S. Györke, D. Terentyev, MCU overexpression evokes disparate dose-dependent effects on mito-ROS and spontaneous $Ca^{2+}$ release in hypertrophic rat cardiomyocytes. *Am. J. Physiol. Heart Circ. Physiol.* **321**, H615–H632 (2021).
18. L. K. Seidlmayer, V. V. Juettner, S. Kettlewell, E. V. Pavlov, L. A. Blatter, E. N. Dedkova, Distinct mPTP activation mechanisms in ischaemia-reperfusion: Contributions of $Ca^{2+}$, ROS, pH, and inorganic polyphosphate. *Cardiovasc. Res.* **106**, 237–248 (2015).
19. D. Ponnalagu, S. G. Rao, J. Farber, W. Xin, A. T. Hussain, K. Shah, S. Tanda, M. Berryman, J. C. Edwards, H. Singh, Molecular identity of cardiac mitochondrial chloride intracellular channel proteins. *Mitochondrion* **27**, 6–14 (2016).
20. K. M. Pinckard, V. K. Shettigar, K. R. Wright, E. Abay, L. A. Baer, P. Vidal, R. S. Dewal, D. das, S. Duarte-Sanmiguel, D. Hernández-Saavedra, P. J. Arts, A. C. Lehnig, V. Bussberg, N. R. Narain, M. A. Kiebish, F. Yi, L. M. Sparks, B. H. Goodpaster, S. R. Smith, R. E. Pratley, E. D. Lewandowski, S. V. Raman, L. E. Wold, D. Gallego-Perez, P. M. Coen, M. T. Ziolo, K. I. Stanford, A novel endocrine role for the BAT-released lipokine 12,13-diHOME to mediate cardiac function. *Circulation* **143**, 145–159 (2021).
21. D. Terentyev, I. Györke, A. E. Belevych, R. Terentyeva, A. Sridhar, Y. Nishijima, E. C. de Blanco, S. Khanna, C. K. Sen, A. J. Cardounel, C. A. Carnes, S. Györke, Redox modification of ryanodine receptors contributes to sarcoplasmic reticulum $Ca^{2+}$ leak in chronic heart failure. *Circ. Res.* **103**, 1466–1472 (2008).
22. A. E. Belevych, D. Terentyev, R. Terentyeva, H. T. Ho, I. Gyorke, I. M. Bonilla, C. A. Carnes, G. E. Billman, S. Györke, Shortened $Ca^{2+}$ signaling refractoriness underlies cellular arrhythmogenesis in a postinfarction model of sudden cardiac death. *Circ. Res.* **110**, 569–577 (2012).
23. E. Gao, Y. H. Lei, X. Shang, Z. M. Huang, L. Zuo, M. Boucher, Q. Fan, J. K. Chuprun, X. L. Ma, W. J. Koch, A novel and efficient model of coronary artery ligation and myocardial infarction in the mouse. *Circ. Res.* **107**, 1445–1453 (2010).
24. A. Kohut, N. Patel, H. Singh, Comprehensive echocardiography assessment of the right ventricle in murine models. *J. Cardiovasc. Ultrasound* **24**, 229 (2016).
25. S. K. Goswami, D. Ponnalagu, A. T. Hussain, K. Shah, P. Karekar, S. G. Rao, A. L. Meredith, M. Khan, H. Singh, Expression and activation of BK$_{Ca}$ channels in mice protects against ischemia-reperfusion injury of isolated hearts by modulating mitochondrial function. *Front. Cardiovasc. Med.* **5**, 194 (2018).
26. J. Yanni, J. O. Tellez, M. Mączewski, U. Mackiewicz, A. Beresewicz, R. Billeter, H. Dobrzynski, M. R. Boyett, Changes in ion channel gene expression underlying heart failure-induced sinoatrial node dysfunction. *Circ. Heart Fail.* **4**, 496–508 (2011).
27. S. Sorota, Insights into the structure, distribution and function of the cardiac chloride channels. *Cardiovasc. Res.* **42**, 361–376 (1999).
28. B. Wojciak-Stothard, V. B. Abdul-Salam, K. H. Lao, H. Tsang, D. C. Irwin, C. Lisk, Z. Loomis, K. R. Stenmark, J. C. Edwards, S. H. Yuspa, L. S. Howard, R. J. Edwards, C. J. Rhodes, J. S. R. Gibbs, J. Wharton, L. Zhao, M. R. Wilkins, Aberrant chloride intracellular channel 4 expression contributes to endothelial dysfunction in pulmonary arterial hypertension. *Circulation* **129**, 1770–1780 (2014).
29. Y. Liu, Z. Wang, M. Li, Y. Ye, Y. Xu, Y. Zhang, R. Yuan, Y. Jin, Y. Hao, L. Jiang, Y. Hu, S. Chen, F. Liu, Y. Zhang, W. Wu, Y. Liu, Chloride intracellular channel 1 regulates the antineoplastic effects of metformin in gallbladder cancer cells. *Cancer Sci.* **108**, 1240–1252 (2017).
30. J. Zhong, X. Kong, H. Zhang, C. Yu, Y. Xu, J. Kang, H. Yu, H. Yi, X. Yang, L. Sun, Inhibition of CLIC4 enhances autophagy and triggers mitochondrial and ER stress-induced apoptosis in human glioma U251 cells under starvation. *PLOS ONE* **7**, e39378 (2012).
31. K. S. Suh, M. Mutoh, K. Nagashima, E. Fernandez-Salas, L. E. Edwards, D. D. Hayes, J. M. Crutchley, K. G. Marin, R. A. Dumont, J. M. Levy, C. Cheng, S. Garfield, S. H. Yuspa,

The organellular chloride channel protein CLIC4/mtCLIC translocates to the nucleus in response to cellular stress and accelerates apoptosis. *J. Biol. Chem.* **279**, 4632–4641 (2004).
32. I. Guillemin, M. Becker, K. Ociepka, E. Friauf, H. G. Nothwang, A subcellular prefractionation protocol for minute amounts of mammalian cell cultures and tissue. *Proteomics* **5**, 35–45 (2005).
33. Y. Yuan, Y. Y. Wang, X. Liu, B. Luo, L. Zhang, F. Zheng, X. Y. Li, L. Y. Guo, L. Wang, M. Jiang, Y. M. Pan, Y. W. Yan, J. Y. Yang, S. Y. Chen, J. N. Wang, J. M. Tang, KPC1 alleviates hypoxia/reoxygenation-induced apoptosis in rat cardiomyocyte cells though BAX degradation. *J. Cell. Physiol.* **234**, 22921–22934 (2019).
34. M. R. Duchen, Mitochondria and calcium: From cell signalling to cell death. *J. Physiol.* **529** (Pt 1), 57–68 (2000).
35. W. Yu, H. Jin, Y. Huang, Mitochondria-associated membranes (MAMs): A potential therapeutic target for treating Alzheimer's disease. *Clin. Sci. (Lond.)* **135**, 109–126 (2021).
36. P. Gao, Z. Yan, Z. Zhu, Mitochondria-associated endoplasmic reticulum membranes in cardiovascular diseases. *Front. Cell Dev. Biol.* **8**, 604240 (2020).
37. D. Ponnalagu, H. Singh, Anion channels of mitochondria. *Handb. Exp. Pharmacol.* **240**, 71–101 (2016).
38. E. Fernández-Salas, K. S. Suh, V. V. Speransky, W. L. Bowers, J. M. Levy, T. Adams, K. R. Pathak, L. E. Edwards, D. D. Hayes, C. Cheng, A. C. Steven, W. C. Weinberg, S. H. Yuspa, mtCLIC/CLIC4, an organellular chloride channel protein, is increased by DNA damage and participates in the apoptotic response to p53. *Mol. Cell. Biol.* **22**, 3610–3620 (2002).
39. R. R. Duncan, P. K. Westwood, A. Boyd, R. H. Ashley, Rat brain p64H1, expression of a new member of the p64 chloride channel protein family in endoplasmic reticulum. *J. Biol. Chem.* **272**, 23880–23886 (1997).
40. G. Csordás, C. Renken, P. Várnai, L. Walter, D. Weaver, K. F. Buttle, T. Balla, C. A. Mannella, G. Hajnóczky, Structural and functional features and significance of the physical linkage between ER and mitochondria. *J. Cell Biol.* **174**, 915–921 (2006).
41. M. S. Herrera-Cruz, T. Simmen, Over six decades of discovery and characterization of the architecture at mitochondria-associated membranes (MAMs). *Adv. Exp. Med. Biol.* **997**, 13–31 (2017).
42. S. Hamilton, R. Terentyeva, R. T. Clements, A. E. Belevych, D. Terentyev, Sarcoplasmic reticulum-mitochondria communication; implications for cardiac arrhythmia. *J. Mol. Cell. Cardiol.* **156**, 105–113 (2021).
43. G. Santulli, R. Nakashima, Q. Yuan, A. R. Marks, Intracellular calcium release channels: An update. *J. Physiol.* **595**, 3041–3051 (2017).
44. B. R. Fruen, P. K. Kane, J. R. Mickelson, C. F. Louis, Chloride-dependent sarcoplasmic reticulum $Ca^{2+}$ release correlates with increased $Ca^{2+}$ activation of ryanodine receptors. *Biophys. J.* **71**, 2522–2530 (1996).
45. X. Meng, G. Wang, C. Viero, Q. Wang, W. Mi, X. D. Su, T. Wagenknecht, A. J. Williams, Z. Liu, C. C. Yin, CLIC2-RyR1 interaction and structural characterization by cryo-electron microscopy. *J. Mol. Biol.* **387**, 320–334 (2009).
46. R. E. Yoast, S. M. Emrich, X. Zhang, P. Xin, V. Arige, T. Pathak, J. C. Benson, M. T. Johnson, A. E. Abdelnaby, N. Lakomski, N. Hempel, J. M. Han, G. Dupont, D. I. Yule, J. Sneyd, M. Trebak, The mitochondrial $Ca^{2+}$ uniporter is a central regulator of interorganellar $Ca^{2+}$ transfer and NFAT activation. *J. Biol. Chem.* **297**, 101174 (2021).
47. Z. Dong, S. Shanmughapriya, D. Tomar, N. Siddiqui, S. Lynch, N. Nemani, S. L. Breves, X. Zhang, A. Tripathi, P. Palaniappan, M. F. Riitano, A. M. Worth, A. Seelam, E. Carvalho, R. Subbiah, F. Jaña, J. Soboloff, Y. Peng, J. Y. Cheung, S. K. Joseph, J. Caplan, S. Rajan, P. B. Stathopulos, M. Madesh, Mitochondrial $Ca^{2+}$ uniporter is a mitochondrial luminal redox sensor that augments MCU channel activity. *Mol. Cell* **65**, 1014–1028.e7 (2017).
48. J. O-Uchi, B. S. Jhun, S. Xu, S. Hurst, A. Raffaello, X. Liu, B. Yi, H. Zhang, P. Gross, J. Mishra, A. Ainbinder, S. Kettlewell, G. L. Smith, R. T. Dirksen, W. Wang, R. Rizzuto, S.-S. Sheu, Adrenergic signaling regulates mitochondrial $Ca^{2+}$ uptake through Pyk2-dependent tyrosine phosphorylation of the mitochondrial $Ca^{2+}$ uniporter. *Antioxid. Redox Signal.* **21**, 863–879 (2014).
49. H. Zhou, S. Wang, S. Hu, Y. Chen, J. Ren, ER-mitochondria microdomains in cardiac ischemia-reperfusion injury: A fresh perspective. *Front. Physiol.* **9**, 755 (2018).
50. R. J. Diaz, A. Hinek, G. J. Wilson, Direct evidence of chloride ion efflux in ischaemic and pharmacological preconditioning of cultured cardiomyocytes. *Cardiovasc. Res.* **87**, 545–551 (2010).
51. R. J. Diaz, K. Fernandes, Y. Lytvyn, K. Hawrylyshyn, K. Harvey, T. Hossain, A. Hinek, G. J. Wilson, Enhanced cell-volume regulation in cyclosporin A cardioprotection. *Cardiovasc. Res.* **98**, 411–419 (2013).
52. H. Xue, J. Lu, R. Yuan, J. Liu, Y. Liu, K. Wu, J. Wu, J. du, B. Shen, Knockdown of CLIC4 enhances ATP-induced HN4 cell apoptosis through mitochondrial and endoplasmic reticulum pathways. *Cell Biosci.* **6**, 5 (2016).
53. T. M. Bauer, E. Murphy, Role of mitochondrial calcium and the permeability transition pore in regulating cell death. *Circ. Res.* **126**, 280–293 (2020).
54. M. Ackers-Johnson, P. Y. Li, A. P. Holmes, S. M. O'Brien, D. Pavlovic, R. S. Foo, A simplified, langendorff-free method for concomitant isolation of viable cardiac myocytes and nonmyocytes from the adult mouse heart. *Circ. Res.* **119**, 909–920 (2016).
55. D. Ponnalagu, S. G. Rao, J. Farber, W. Xin, A. T. Hussain, K. Shah, S. Tanda, M. A. Berryman, J. C. Edwards, H. Singh, Data supporting characterization of CLIC1, CLIC4, CLIC5 and DmCLIC antibodies and localization of CLICs in endoplasmic reticulum of cardiomyocytes. *Data Brief* **7**, 1038–1044 (2016).
56. B. G. Hughes, X. Fan, W. J. Cho, R. Schulz, MMP-2 is localized to the mitochondria-associated membrane of the heart. *Am. J. Physiol. Heart Circ. Physiol.* **306**, H764–H770 (2014).
57. A. Belevych, Z. Kubalova, D. Terentyev, R. L. Hamlin, C. A. Carnes, S. Györke, Enhanced ryanodine receptor-mediated calcium leak determines reduced sarcoplasmic reticulum calcium content in chronic canine heart failure. *Biophys. J.* **93**, 4083–4092 (2007).

**Acknowledgments:** We thank J. Kandola for her help with the blinded analysis of the data. We also thank Lifeline of Ohio and the OSU Department of Surgery for their collaborations in providing nonfailing and failing cardiac tissue. **Funding:** H.S. was supported by the National Heart, Lung, and Blood Institute (HL133050 and HL157453) and the American Heart Association–Transformational Project Award (965301), and D.P. was supported by AHA-Career Development Award (20CDA35310714) grant. T.J.H. was supported by the National Heart, Lung, and Blood Institute (HL156652, HL135096, and HL134824). M.K. was supported by HL136232, and L.E.W. was supported by HL139348 and AG057046. D.T. was supported by HL142588 and HL121796. S.H. was supported by The Ohio State University President's Postdoctoral Scholars Award and 1K99HL155492. S.S.B. was supported by HL132123 and HL153164. **Author contributions:** D.P. and H.S. conceptualized the project and obtained funding for the research work. D.P. wrote the manuscript. D.P., S.H., S.S., D.A., N.S., I.H., and H.S. performed experiments and analyzed data. X.X. and E.G. performed surgeries for the manuscript. D.T., J.C.E., S.S.B., L.E.W., T.J.H., P.M.L.J., M.K., A.R.K., and W.J.K. provided resources and facilities. All authors reviewed and revised the manuscript. **Competing interests:** The authors declare that they have no competing interests. **Data and materials availability:** All data needed to evaluate the conclusions in the paper are present in the paper and/or the Supplementary Materials.

Submitted 14 January 2022
Accepted 25 August 2022
Published 21 October 2022
10.1126/sciadv.abo1244